

# Chapter 4

## Sedimentation of Particulate Systems

**Abstract** This chapter deals with sedimentation of particulate systems considered as discrete media. Sedimentation is the settling of a particle or suspension of particles in a fluid due to the effect of an external force such as gravity, centrifugal force or any other body force. Discrete sedimentation has been successful in establishing constitutive equations for continuous sedimentation processes. The foundation of the motion of particles in fluids is discussed in different flow regimes, Euler's flow, Stokes flow and flows with a boundary layer. Starting from the sedimentation of a sphere in an unbounded fluid, a complete analysis is made of the settling of individual spherical particles and suspensions. The results are extended to isometric particles and to arbitrarily shaped particles. Sphericity as a shape factor is used to describe the form of isometric particles. A hydrodynamic sphericity must be defined for particles with arbitrary shapes by performing sedimentation or fluidization experiments, calculating the drag coefficient for the particles using the volume equivalent diameter and obtaining a sphericity defined for isometric particles that fits experimental values. A modified drag coefficient and sedimentation velocities permits grouping all sedimentation results in one single equation for particles of any shape.

*Sedimentation* is the settling of a particle, or suspension of particles, in a fluid due to the effect of an external force such as gravity, centrifugal force or any other body force. For many years, workers in the field of Particle Technology have been looking for a simple equation relating the settling velocity of particles to their size, shape and concentration. Such a simple objective has required a formidable effort and it has been solved, only in part, through the work of Newton (1687) and Stokes (1844) on flow around a particle, and the more recent research of Lapple (1940), Heywood (1962), Batchelor (1967), Zenz (1966), Barnea and Mitzrahi (1973) and many others, to those Turton and Levenspiel (1986) and Haider and Levenspiel (1998). Concha and collaborators established in 1979 an heuristic theory of sedimentation, that is, a theory based on the fundamental principles of mechanics, but to a greater or lesser degree to intuition and empirism. These works, (Concha and Almendra 1979a, b; Concha and Barrientos 1982, 1986; Concha and Christiansen 1986), first solve the settling of one particle in a fluid, then, they introduce

corrections for the interaction between particles, through which the settling velocity of a suspension is drastically reduced. Finally, the settling of isometric and non-spherical particles was treated. This approach, which uses principles of particle mechanics, receives the name of the *discrete approach* to sedimentation, or *discrete sedimentation*.

Discrete sedimentation has been successful in establishing constitutive equations in processes using sedimentation in order to analyze the sedimentation properties of a certain particulate material in a given fluid. Nevertheless, to analyze a sedimentation process and to obtain behavioral pattern permitting the prediction of capacities and equipment design procedures, another approach is required, the so-called *continuum approach*. In the present chapter the discrete approach will be analyzed, leaving the continuum approach for later chapters.

## 4.1 Discrete Sedimentation

The physics underlying sedimentation, that is, the settling of a particle in a fluid has long been known. Stokes showed the equation describing the sedimentation of a sphere in 1851 and that can be considered as the starting point of all discussions of the sedimentation process. Stokes showed that the settling velocity of a sphere in a fluid is directly proportional to the square of the particle radius, to the gravitational force and to the density difference between solid and fluid, and inversely proportional to fluid viscosity. This equation is based on a force balance around the sphere. Nevertheless, the proposed equation is valid only for slow motions, so that in other cases expressions that are more elaborate should be used. The problem is related to the hydrodynamic force between the particle and the fluid.

Consider the incompressible flow of a fluid around a solid sphere. The equations describing the phenomena are the continuity equation and Navier–Stokes equation:

$$\nabla \cdot \mathbf{v} = 0$$

$$\rho \left( \frac{\partial \mathbf{v}}{\partial t} + \nabla \mathbf{v} \cdot \mathbf{v} \right) = -\nabla p + \mu \nabla^2 \mathbf{v} + \rho \mathbf{g}$$
(4.1)

where  $\mathbf{v}$  and  $p$  are the fluid velocity and pressure field,  $\rho$  and  $\mu$  are the fluid density and viscosity and  $\mathbf{g}$  is the gravity force vector.

Unfortunately, Navier–Stokes equation are non-linear and it is impossible to be solved explicitly in a general form. Therefore, methods have been used to solve it in special cases. It is known that the Reynolds number  $Re = \rho_f d u / \mu$ , where  $\rho_f$ ,  $d$  and  $u$  are the fluid density and the particle diameter and velocity respectively, is an important parameter that characterizes the flow. It is a dimensionless number representing the ratio of convective to diffusive forces in Navier–Stokes equation. In dimensionless form, Navier–Stokes equation becomes:

$$\frac{1}{St} \frac{\partial \mathbf{v}^*}{\partial t^*} + \nabla^* \mathbf{v}^* \cdot \mathbf{v}^* = -\frac{1}{Ru} \nabla^* p^* + \frac{1}{Re} \nabla^{*2} \mathbf{v}^* - \frac{1}{Fr} \mathbf{e}_k \quad (4.2)$$

where the starred terms represent dimensionless variables defined by:  $\mathbf{v}^* = \mathbf{v}/u_0$ ;  $p^* = p/p_0$ ;  $t^* = t/t_0$ ;  $\nabla^* = L\nabla$  and  $u_0$ ,  $p_0$ ,  $t_0$  and  $L$  are characteristic velocity, pressure and time and length in the problem, and  $St$ ,  $Ru$ ,  $Re$  and  $Fr$  are the Struhal, Ruark, Reynolds and Froude numbers and  $\mathbf{e}_k$  is the vertical unit vector:

$$\text{Strouhal } St = \frac{t_0 u_0}{L} \quad (4.3)$$

$$\text{Ruark } Ru = \frac{\rho u_0^2}{p_0} \quad (4.4)$$

$$\text{Reynolds } Re = \frac{\rho u_0 L}{\mu} \quad (4.5)$$

$$\text{Froude } Fr = \frac{u_0^2}{Lg} \quad (4.6)$$

When the Reynolds number is small ( $Re \rightarrow 0$ ), for example  $Re < 10^{-3}$ , convective forces may be neglected in Navier–Stokes equation, obtaining the so called *Stokes Flow*. In dimensional form Stokes Flow is represented by:

$$\begin{aligned} \nabla \cdot \mathbf{v} &= 0 \\ \rho \frac{\partial \mathbf{v}}{\partial t} &= -\nabla p + \mu \nabla^2 \mathbf{v} + \rho \mathbf{g} \end{aligned} \quad (4.7)$$

### 4.1.1 Hydrodynamic Force on a Sphere in Stokes Flow

Due to the linearity of the differential equation in Stokes Flow, the velocity, the pressure and the *hydrodynamic force* in a steady flow are linear functions of the relative solid–fluid velocity. For the hydrodynamic force, the linear function, depends on the size and shape of the particle ( $6\pi R$  for the sphere) and on fluid viscosity ( $\mu$ ). Solving the boundary value problem, and neglecting the Basset term of added mass, yields (Happel and Brenner 1965) for a sphere:

$$F_D = -6\pi\mu Ru \quad (4.8)$$

It is common to write the hydrodynamic force in its dimensionless form known as *drag coefficient*  $C_D$ :

$$C_D = \frac{F_D}{(1/2\rho_f u^2)(\pi R^2)} \quad (4.9)$$

where  $\rho_f$  is the fluid density. Substituting (4.9) into (4.8), the drag coefficient on a sphere in Stokes flow is:

$$C_D = \frac{24}{Re} \quad (4.10)$$

#### 4.1.2 Macroscopic Balance on a Sphere in Stokes Flow

Consider a small solid sphere submerged in a viscous fluid and suspended with a string. If the sphere, with density greater than that of the fluid, is in equilibrium, the balance of forces around it is zero. The forces acting on the particles are: (1) gravity  $F_g$ , that pulls the sphere down, (2) buoyancy  $F_b$ , that is, the pressure forces of the fluid acting on the particle that pushes the sphere upwards and (3) the string resistance  $F_{string}$ , that supports the particle from falling, see Fig. 4.1. The force balance gives:

$$0 = F_{string} + \underbrace{F_g}_{-\rho_p V_p g} + \underbrace{F_b}_{+\rho_f V_p g} \quad (4.11)$$

$$0 = F_{string} - \rho_p V_p g + \rho_f V_p g \quad (4.12)$$

$$F_{string} = \underbrace{(\rho_p - \rho_f)}_{\Delta\rho} V_p g \equiv \Delta\rho V_p g \quad (4.13)$$

If the string is cut, forces become unbalanced and, according to Newton's second Law, the particle will accelerate. The initial acceleration can be obtained from the new force balance, where the string resistance is absent. Figure 4.2 shows this new force balance before the motion begins.

The initial acceleration is:

$$\begin{aligned} \rho_p V_p a(t=0) &= \Delta\rho V_p g \\ a(t=0) &= \frac{\Delta\rho}{\rho_p} g \end{aligned} \quad (4.14)$$

**Fig. 4.1** Equilibrium of a sphere submerged in a viscous fluid

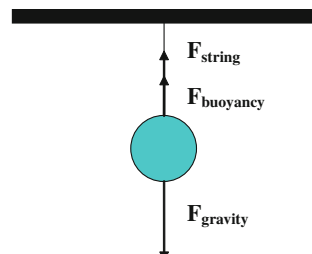
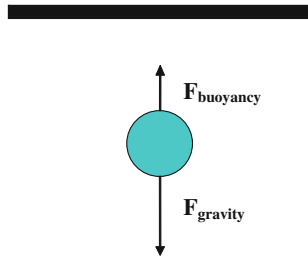


**Fig. 4.2** State before the motion initiates



Once the particle is in motion, a new force, the drag, appears representing the resistance opposed by the fluid to the particle motion. This force  $F_D$  is proportional to the relative solid–fluid velocity and to the relative particle acceleration. Since the fluid is at rest, it corresponds to the sphere velocity and acceleration. Once the motion starts, the drag force is added and the balance of forces becomes, Fig. 4.3:

$$\rho_p V_p a(t) = \underbrace{\Delta\rho V_p g}_{\text{Netweight}} - \underbrace{6\pi\mu R u(t) - (1/2)\rho_p V_p a(t)}_{\text{Dragforce}} \quad (4.15)$$

$$\frac{3}{2} \rho_p V_p a(t) = \Delta\rho g V_p - 6\pi\mu R u(t) \quad (4.16)$$

The term  $(1/2)\rho_p V_p$  that was added to the mass  $\rho_p V_p$  in the first term of Eq. (4.16) is called *added mass* induced by the acceleration.

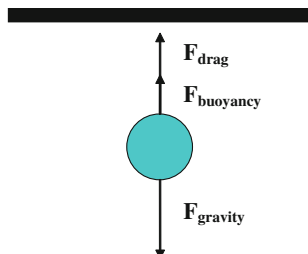
Due to the increase in the velocity  $u(t)$  with time, the sum of the first and last term of Eq. (4.16) diminishes, becoming zero at a given time. At that time, the velocity becomes a constant called *terminal velocity*  $u = u_\infty$ , which is a characteristic of the solid–fluid system. From (4.16) with  $a(t) = 0$ ,

$$u_\infty = \frac{2}{9} \frac{\Delta\rho R^2 g}{\mu} = \frac{1}{18} \frac{\Delta\rho d^2 g}{\mu} \quad (4.17)$$

This expression receives the name of *Stokes Equation* and is valid for small Reynolds numbers.

**Problem 4.1** Calculate the terminal sedimentation velocity of a quartz sphere with a diameter of 10  $\mu\text{m}$  and 2.65  $\text{g}/\text{cm}^3$  in density in water at 20 °C.

**Fig. 4.3** State after the motion starts



The water viscosity at 20 °C is 0.01 g/cm s, then, applying Eq. (4.17) results in:

$$u_{\infty} = \frac{1}{18} \frac{(2,650 - 1,000) \times (10/1,000,000)^2 \times 9.81}{0.001} = 5.00 \times 10^{-6} \text{ m/s.}$$

## Sedimentation dynamics

Equation (4.16) is the differential equation for the settling velocity of a sphere in a gravity field. It can be written in the form:

$$\dot{u}(t) + \frac{2}{3} \frac{\mu}{18\rho_p d^2} u(t) - \frac{2\Delta\rho}{3\rho_p} g = 0 \quad (4.18)$$

$$\text{Its solution is: } u(t) = \frac{1}{18} \frac{\Delta\rho d^2 g}{\mu} \left( 1 - \exp\left(-\frac{2}{3} \frac{\mu}{18\rho_p d^2} t\right) \right) \quad (4.19)$$

The term inside the exponential term multiplying the time  $t$  is called the *Stokes Number* and the term outside the parenthesis is the *terminal velocity*, as we already saw in (4.17).

**Problem 4.2** Calculate the terminal settling velocity and the time to reach it for quartz particles, 10, 50 and 100 µm in size and 2.65 g/cm<sup>3</sup> in density, in water at 20 °C.

Applying Eqs. (4.19) and (4.17), the values of terminal velocities of 0.899, 0.225 and 0.00899 cm/s and times of 0.03140, 0.00740 and 0.00030 are obtained for particles with diameters of  $d = 100, 50$  and 10 µm respectively. Figure 4.4 shows the evolution of the particle velocities.

### 4.1.3 Hydrodynamic Force on a Sphere in Euler's Flow

When the Reynolds number tends to infinity ( $Re \rightarrow \infty$ ), viscous forces disappear and Navier–Stokes equation becomes *Euler's Equation for Inviscid Flow*.

$$\begin{aligned} \nabla \cdot \mathbf{v} &= 0 \\ \rho \frac{\partial \mathbf{v}}{\partial t} \nabla \cdot \mathbf{v} &= -\nabla p + \rho \mathbf{g} \end{aligned} \quad (4.20)$$

In this case, the tangential component of the velocity at the particle surface is also a linear function of the relative solid–fluid velocity, but the radial component is equal to zero:

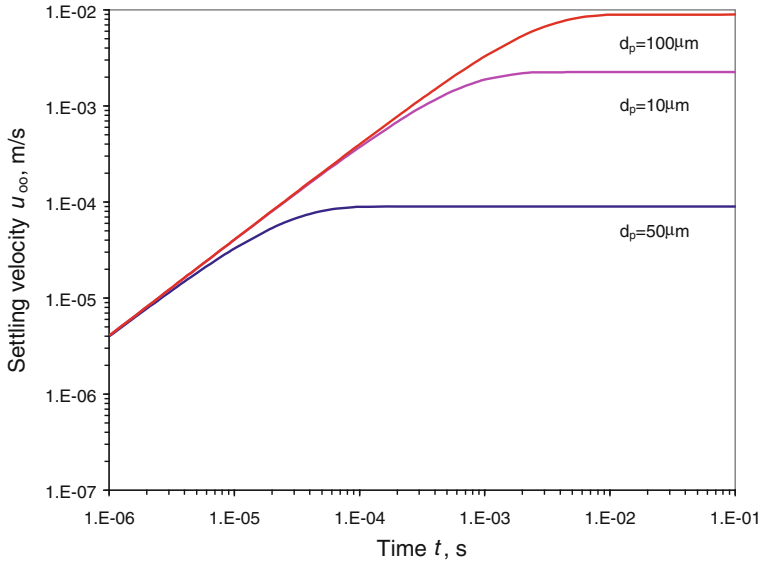


**Fig. 4.4** Settling velocity versus time for Problem 4.2

$$u_\theta(\theta) = \left( \frac{3}{2} \sin \theta \right) u \quad \text{and} \quad u_r = 0 \quad (4.21)$$

Now, the pressure is given by a non-linear function called the *Bernoulli equation* (Batchelor 1967):

$$\begin{aligned} p(\theta) + 1/2 \rho_f u_\theta^2 &= p + 1/2 \rho_f u^2 = \text{constant} \\ p(\theta) - p &= \frac{1}{2} \rho_f u^2 \left( 1 - \left( \frac{u_\theta}{u} \right)^2 \right) \end{aligned} \quad (4.22)$$

Substituting (4.21) into (4.22), the dimensionless pressure, called *pressure coefficient*, defined by  $C_p = (p(\theta) - p)/(1/2)\rho_f u^2$ , may be expressed in Euler's flow by:

$$C_p = 1 - \frac{9}{2} \sin^2 \theta \quad (4.23)$$

Figure 4.5 shows Eq. (4.23) in graphic form, where  $p(\theta)$  and  $u_\theta$  are respectively the pressure and tangential velocity at an angle  $\theta$  on the surface of the sphere, and  $p$  and  $u$  are the values of the same variables at the bulk of the flow.

For an inviscid stationary flow, the hydrodynamic force is zero. This result is due to the fact that the friction drag is zero in the absence of viscosity and that the form drag depends on the pressure distribution over the surface of the sphere and this distribution is symmetric, leading to a zero net force.

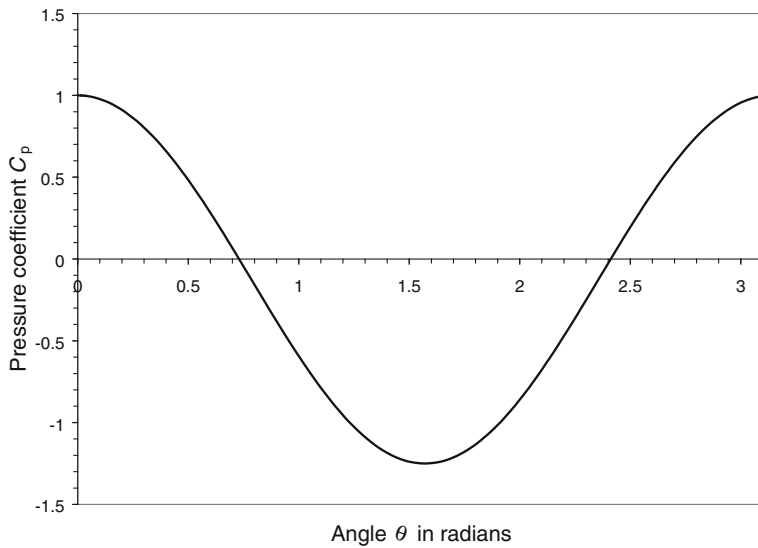


**Fig. 4.5** Pressure coefficient in terms of the distance over the sphere in an inviscid flow (Schlichting 1968, p. 21)

#### 4.1.4 Hydrodynamic Force on a Sphere in Prandtl's Flow

For intermediate values of the Reynolds Number, inertial and viscous forces in the fluid are of the same order of magnitude. In this case, the flow may be divided into two parts, an external inviscid flow far from the particle and an internal flow near the particle, where viscosity plays an important role. This picture forms the basis of the *Boundary-Layer Theory* (Meksyn 1961; Rosenhead 1963; Golstein 1965; Schlichting 1968).

In the external inviscid flow, Euler's equations are applicable and the velocity and pressure distribution may be obtained from Eqs. (4.21) and (4.23). The region of viscous flow near the particle is known as the *boundary layer* and it is there where a steep velocity gradient permits the non-slip condition at the solid surface to be satisfied. The energy dissipation produced by the viscous flow within the boundary layer retards the flow and, at a certain point, aided by the adverse pressure gradient, the flow reverses its direction. These phenomena force the fluid particles outwards and away from the solid producing the phenomena called *boundary layer separation*, which occurs at an *angle of separation* given by Lee and Barrow (1968):

$$\theta_s = 214 Re^{-0.1} \quad \text{for } 24 < Re < 10,000 \quad (4.24)$$

For  $Re = 24$  the value of the angle of separation is  $\theta_s = 155.7$  diminishing to  $\theta_s = 85.2$  for  $Re = 10,000$ . For Reynolds numbers exceeding 10,000, the angle of separation diminishes slowly from  $\theta_s = 85.2^\circ$  to  $84^\circ$  and then maintains this value

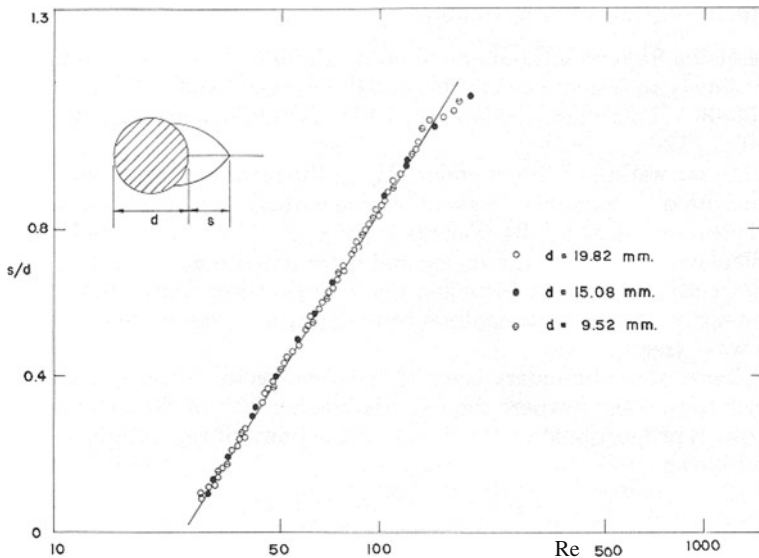


**Fig. 4.6** Length of the region of closed streamlines behind a sphere (from Taneda 1956; Batchelor 1967, p. 262)

up to  $Re \approx 150,000$  (Tomotika 1936; Fage 1937; Amai 1938; Cabtree et al. 1963). Due to the separation of the boundary layer, the region of closed streamlines behind the sphere contains a standing ring-vortex, which first appears at Reynolds number of  $Re \approx 24$ . See Fig. 4.6.

Taneda (1956) determined that beyond  $Re \approx 130$  the ring-vortex began to oscillate and that at higher Reynolds numbers the fluid in the region of closed streamlines broke away and was carried downstream forming a wake. Figure 4.7 shows a similar case for the flow around a cylinder.

The thickness “ $\delta$ ” of the boundary layer, defined as the distance from the solid surface to the region where the tangential velocity  $v_\theta$  reaches 99 % of the value of the external inviscid flow, is proportional to  $Re^{-0.5}$  and, at the point of separation, may be written in the form:

$$\frac{\delta}{R} = \frac{\delta_0}{Re^{1/2}} \quad (4.25)$$

McDonald (1954) gives a value of  $\delta_0 = 9.06$ .

The separation of the boundary layer prevents the recovery of the pressure at the rear of the sphere, resulting in an asymmetrical pressure distribution with a higher pressure at the front of the sphere. Figure 4.8 shows the pressure coefficient of a sphere in terms of the distance from the front stagnation point over the surface of the sphere in an inviscid flow and in boundary layer flow. The figure shows that the pressure has an approximate constant value behind the separation point at Reynolds numbers around  $Re \approx 150,000$ . This dimensionless pressure is called

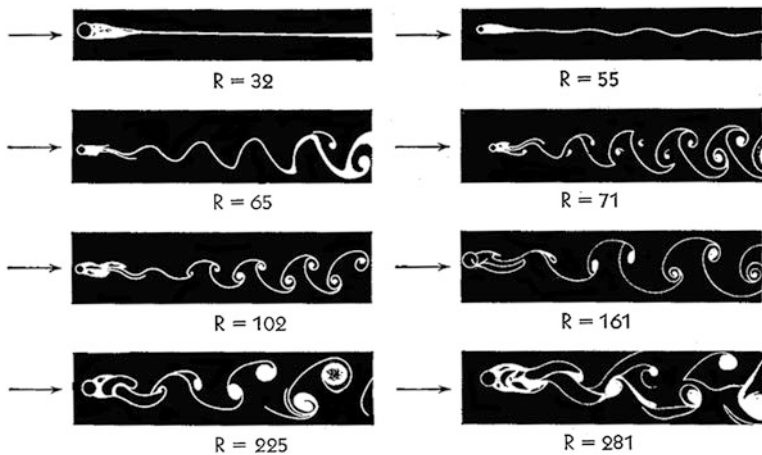
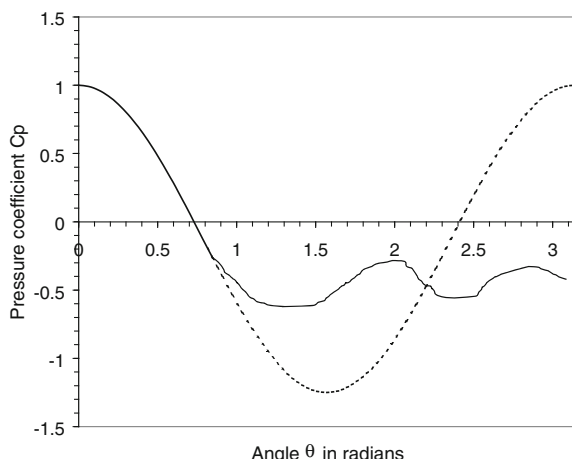


**Fig. 4.7** Flow around a cylinder for several values of the Reynolds number

base pressure and has a value of  $p_b^* \approx -0.4$  (Fage 1937; Lighthill 1963, p. 108; Goldstein 1965, pp. 15 and 497; Schlichting 1968, p. 21).

The asymmetry of the pressure distribution explains the origin of the form-drag, the magnitude of which is closely related to the position of the point of separation. The farther the separation points from the front stagnation point, the smaller the form-drag. For a sphere at high Reynolds numbers, from  $Re = 10,000$  up to  $Re = 150,000$ , the position of the separation point does not change very much, except with the change of flow from laminar to turbulent. Therefore, the *form-drag* will remain approximately constant. At the same time, the *friction-drag*, also called *skin friction*, falls proportionally to  $Re^{-1/2}$ . From these observations, we can conclude that, for Reynolds numbers of about  $Re = 1,000$ , the viscous interaction force has diminished sufficiently for its contribution to the total interaction force to

**Fig. 4.8** Pressure coefficient as a function of the distance from the front stagnation point over the surface of a sphere in an inviscid and a boundary layer flow



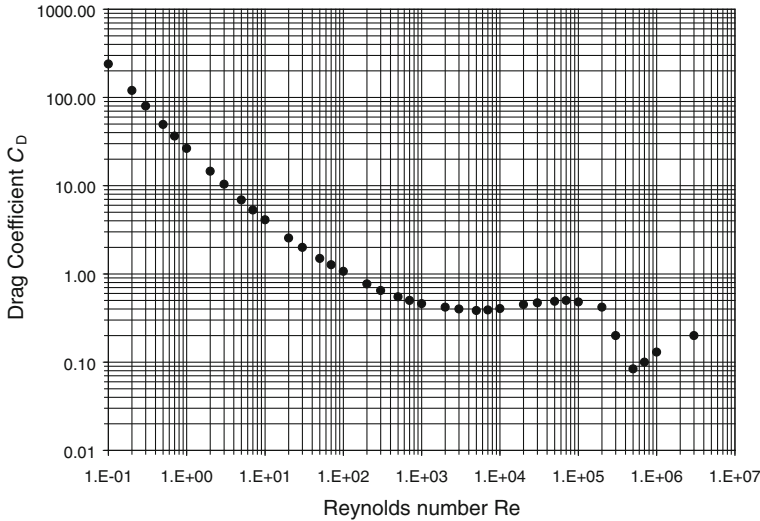


**Fig. 4.9** Drag coefficient  $C_D$  versus Reynolds number, according to standard data from Lapple and Shepherd (1940). See also Perry (1963, p. 561)

be negligible. Therefore, between  $Re \approx 10,000$  to  $Re \approx 150,000$ , the drag coefficient is approximately constant at  $C_D \approx 0.44$ .

For Reynolds numbers greater than  $Re \approx 150,000$ , the flow changes in character and the boundary layer becomes turbulent. The increase in kinetic energy of the external region permits the flow in the boundary layer to reach further to the back of the sphere, shifting the separation point to values close to  $\theta_S \approx 110^\circ$  and permitting also the base pressure to rise. The effect of these changes on the drag coefficient is a sudden drop and after that, a sharp increase with the Reynolds number. Figure 4.9 shows a plot of standard experimental values of the drag coefficient versus the Reynolds number (Lapple and Shepherd 1940), where this effect is shown.

#### 4.1.5 Drag Coefficient for a Sphere in the Range $0 < Re < 150,000$

Figure 4.9 shows the variation of the drag coefficient of a sphere for different values of the Reynolds number, and confirms that for  $Re \rightarrow 0$ ,  $C_D \propto Re^{-1/2}$  and that for  $Re > 1,000$ ,  $C_D \rightarrow 0.43$ . To obtain a general equation relating the drag coefficient to the Reynolds number, we will use the concept of the *boundary layer* and the knowledge that, for a given position at the surface of the sphere, the pressure inside the boundary layer is equal to the pressure in the inviscid region just outside the boundary layer before the separation point, and is a constant

beyond it. We should also remember that the point of separation and the base pressure are constant for Reynolds numbers greater than  $Re \approx 1,000$ .

Consider a solid sphere of radius  $R$  with an attached boundary layer of thickness  $\delta$  submerged in a flow at high Reynolds number (Abraham 1970). Assume that the system of sphere and boundary layer has a spherical shape with a radius equal to  $a$ , which can be approximated by  $a = R + \delta$ , as shown in Fig. 4.10 (Abraham 1970; Concha and Almendra 1979a, b).

Outside the spherical shell of radius  $a$ , and up to the point of separation  $\theta = \theta_s$ , the flow is inviscid and therefore the fluid velocity and the pressure distributions are given by:

$$u_\theta(\theta) = \frac{3}{2}u \sin \theta, \quad \text{for } 0 \leq \theta \leq \theta_s \quad (4.26)$$

$$p(\theta) = \frac{1}{2}\rho_f u^2 \left(1 - \left(\frac{u_\theta}{u}\right)^2\right), \quad \text{for } 0 \leq \theta \leq \theta_s \quad (4.27)$$

Beyond the separation point, a region exists where the pressure is constant and equal to the base pressure  $p_b$ :

$$p(\theta) = p_b, \quad \text{for } \theta_s \leq \theta \leq \pi \quad (4.28)$$

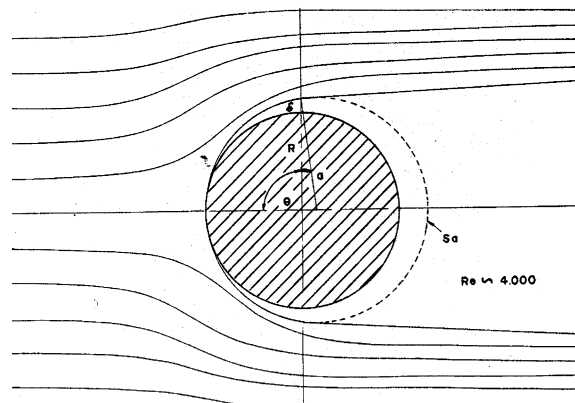
Since the effect of viscosity is confined to the interior of the sphere of radius  $a$ , the total drag exerted by the fluid on  $a$ , consists of a form drag only, Then:

$$F_D = \oint_{S_a} p(\theta) \cos \theta dS \quad (4.29)$$

The element of surface of the sphere of radius  $a$  is:

$$dS = a^2 \sin \theta d\theta d\phi \quad (4.30)$$

**Fig. 4.10** Physical model for the flow in the boundary layer around a sphere (Concha and Almendra 1979a, b)



where  $\phi$  is the azimuthally coordinate. Replacing (4.30) into (4.29) results in:

$$F_D = \int_0^{2\pi} \int_0^\pi p(\theta) \sin \theta \cos \theta d\theta d\phi = 2\pi a^2 \int_0^\pi p(\theta) \sin \theta \cos \theta d\theta$$

Since the values of  $p(\theta)$  are different before and after the separation point, the integrals are separated into two parts, from 0 to  $\theta_s$  and from  $\theta_s$  to  $\pi$ :

$$F_D = 2\pi a^2 \left( \int_0^{\theta_s} p(\theta) \sin \theta d(\sin \theta) + \int_{\theta_s}^\pi p(\theta) \sin \theta d(\sin \theta) \right)$$

Substituting the values of  $p(\theta)$  from (4.27) and (4.28), and integrating the previous equation we obtain:

$$F_D = \pi a^2 \rho_f u^2 \left( \frac{1}{2} \sin^2 \theta_s - \frac{9}{16} \sin^4 \theta_s - \frac{1}{2} p_b^* \sin^2 \theta_s \right) \quad (4.31)$$

Substituting  $a = R + \delta$  and defining the function  $f(\theta_s, p_b^*)$  in the form:

$$f(\theta_s, p_b^*) = \frac{1}{2} \sin^2 \theta_s - \frac{9}{16} \sin^4 \theta_s - \frac{1}{2} p_b^* \sin^2 \theta_s \quad (4.32)$$

we can into (4.31) we can write:

$$F_D = \rho_f u^2 \pi R^2 \left( 1 + \frac{\delta}{R} \right)^2 f(\theta_s, p_b^*) \quad (4.33)$$

In terms of the drag coefficient we have:

$$C_D = 2f(\theta_s, p_b^*) \left( 1 + \frac{\delta}{R} \right)^2 \quad (4.34)$$

and defining the new parameter  $C_0$  in the form:

$$C_0 = 2f(\theta_s, p_b^*) \quad (4.35)$$

Using Eq. (4.32) we obtain:

$$C_D = C_0 \left( 1 + \frac{\delta_0}{Re^{1/2}} \right)^2 \quad (4.36)$$

Calculating the value of  $f(\theta_s, p_b^*)$  for  $\theta_s = 84^\circ$  and  $p_b^* \approx -0.4$ , we obtain  $f(84, -0.4) = 0.142$  and from (4.35)  $C_0 = 0.284$ . Using the value of  $\delta_0 = 9.06$ , we finally obtain:

$$C_D = 0.284 \left( 1 + \frac{9.06}{Re^{1/2}} \right)^2 \quad (4.37)$$

Expression (4.37) represents the drag coefficient for a sphere in boundary layer flow (Concha and Almendra 1979a, b). A comparison with experimental data from Lapple and Shepherd (1940) is shown in Fig. 4.11.

Several alternative empirical equations have been proposed for the drag coefficient of spherical particles. See earlier articles reviewed by Concha and Almendra (1979a, b), Zigrang and Sylvester (1981), Turton and Levenspiel (1986), Turton and Clark (1987), Haider and Levenspiel (1998), and the more recent work of Ganguly (1990), Thomson and Clark (1991), Ganser (1993), Flemmer et al. (1993), Darby (1996), Nguyen et al. (1997), Chabra et al. (1999) and Tsakalakis and Stamboltzis (2001).

It is worthwhile to mention the work of Brauer and Sucker (1976):

$$C_D = 0.49 + \frac{24}{Re} + \frac{3.73}{Re^{1/2}} - \frac{4.83 \times 10^{-3} Re^{1/2}}{1 + 3.0 \times 10^{-6} Re^{3/2}} \quad (4.38)$$

and that of Haider and Levenspiel (1998):

$$C_D = \frac{24}{Re} (1 + 0.1806 Re^{0.6459}) + \frac{0.4251}{1 + 6,880.95/Re} \quad (4.39)$$

who presented an alternative empirical equation for the drag coefficient of spherical particles in the range of Reynolds numbers less than 260,000. Both Eqs.

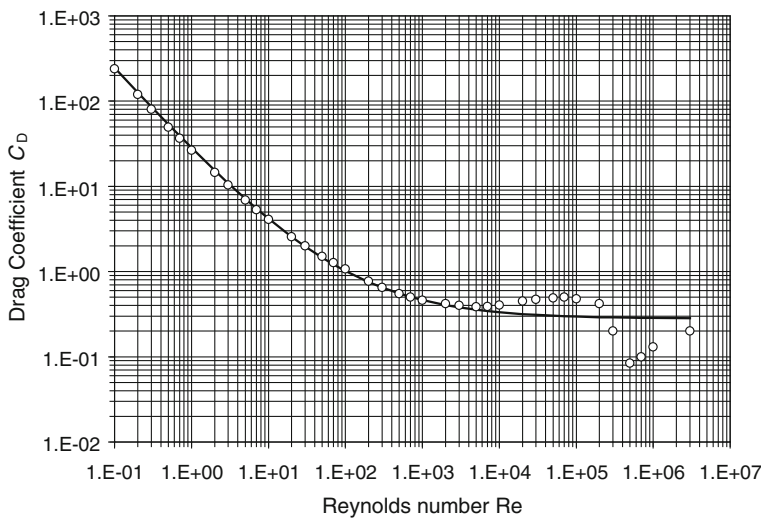


**Fig. 4.11** Drag coefficient versus Reynolds number for a sphere. The continuous line is a simulation of Eq. (4.37). Circles are standard data from Lapple and Shepherd (1940) see Table 4.1

(4.38) and (4.39) give better approximations than Concha and Almendra's equation (4.37) for Reynolds numbers in the range of  $5 \times 10^3 < Re < 5 \times 10^5$ .

Table 4.1 gives the standard drag coefficient of Lappel and Shepherd (1940), L&Sh in table and results of Concha and Almendra (1979a, b), Heider and Levenspiel (1998), H&L in Table 4.1 and Brauer and Sucker (1976), B&Z in Table 4.1 (Fig. 4.12).

#### 4.1.6 Sedimentation Velocity of a Sphere

We have seen that when a particle settles at terminal velocity  $u_\infty$ , a balance is established between drag force, gravity and buoyancy:

$$\begin{aligned} F_{\text{drag}} + F_{\text{gravity}} + F_{\text{buoyancy}} &= 0 \\ F_{\text{drag}} &= -(F_{\text{gravity}} + F_{\text{buoyancy}}) \equiv \text{net weight of the particle} \\ F_D &= -(\rho_p V_p(-g) + \rho_f V_p g) \equiv \Delta\rho V_p g \end{aligned} \quad (4.40)$$

In (4.40)  $\Delta\rho = \rho_s - \rho_f$  is the solid–fluid density difference. This equation shows that the drag force for a particle in sedimentation is known beforehand once the volume of particle and its density difference to the fluid are known. For a spherical particle,  $V_p = 4/3\pi R^3$ , so that:

$$F_D = \frac{4}{3}\pi R^3 \Delta\rho g \quad (4.41)$$

and the drag coefficient:

$$C_D = \frac{F_D}{1/2\rho_f u_\infty^2 \pi R^2} \equiv \frac{4 \Delta\rho d g}{3 \rho_f u_\infty^2} \quad (4.42)$$

where the sphere diameter is  $d = 2R$  and  $u_\infty$  is the terminal settling velocity of a sphere in an infinite fluid.

Since the Reynolds number for the motion of one particle in an infinite fluid is defined by:

$$Re_\infty = \frac{du_\infty \rho_f}{\mu_f}, \quad (4.43)$$

combining it with the drag coefficient yields two dimensionless numbers (Heywood 1962):

$$C_D Re_\infty^2 = \left( \frac{4 \Delta\rho \rho_f g}{3 \mu_f^2} \right) d^3 \quad \frac{Re_\infty}{C_D} = \left( \frac{3 \rho_f^2}{4 \Delta\rho \mu_f g} \right) u_\infty^3 \quad (4.44)$$

**Table 4.1** Drag coefficient versus Reynolds number and dimensionless velocity versus dimensionless diameter

L&Sh	Re	C <sub>D</sub>	C <sub>D</sub> Re <sup>2</sup>	Re/C <sub>D</sub>	d* = (C <sub>D</sub> Re <sup>2</sup> ) <sup>1/3</sup>	u* = (Re/C <sub>D</sub> ) <sup>1/3</sup>	Concha and Almendra		H&L		B&Z
							C <sub>D</sub> sim	d* sim	u* sim	C <sub>D</sub> sim	C <sub>D</sub> sim
	1.000E-01	2.400E+02	2.400E+00	4.167E-04	1.339E+00	7.469E-02	2.462E+02	1.000E-01	4.345E-04	2.498E+02	2.523E+02
	2.000E-01	1.200E+02	4.800E+00	1.667E-03	1.687E+00	1.186E-01	1.265E+02	2.000E-01	1.733E-03	1.277E+02	1.288E+02
	3.000E-01	8.000E+01	7.200E+00	3.750E-03	1.931E+00	1.554E-01	8.615E+01	3.000E-01	3.887E-03	8.664E+01	8.730E+01
	5.000E-01	4.950E+01	1.238E+01	1.010E-02	2.313E+00	2.162E-01	5.342E+01	4.000E-01	6.882E-03	5.354E+01	5.376E+01
	7.000E-01	3.650E+01	1.789E+01	1.918E-02	2.615E+00	2.677E-01	3.918E+01	5.000E-01	1.071E-02	3.920E+01	3.923E+01
	1.000E+00	2.650E+01	2.650E+01	3.774E-02	2.981E+00	3.354E-01	2.834E+01	6.000E-01	1.534E-02	2.833E+01	2.822E+01
	2.000E+00	1.460E+01	5.840E+01	1.370E-01	3.880E+00	5.155E-01	1.536E+01	7.000E-01	2.077E-02	1.539E+01	1.512E+01
	3.000E+00	1.040E+01	9.360E+01	2.885E-01	4.540E+00	6.607E-01	1.087E+01	8.000E-01	2.697E-02	1.094E+01	1.064E+01
	5.000E+00	6.900E+00	1.725E+02	7.246E-01	5.567E+00	9.892E-01	7.146E+00	9.000E-01	3.393E-02	7.252E+00	6.947E+00
	7.000E+00	5.300E+00	2.597E+02	1.321E+00	6.380E+00	1.097E+00	5.481E+00	1.000E+00	4.162E-02	5.605E+00	5.316E+00
	1.000E+01	4.100E+00	4.100E+02	2.439E+00	7.429E+00	1.346E+00	4.183E+00	1.100E+00	5.003E-02	4.319E+00	4.054E+00
	2.000E+01	2.550E+00	1.920E+03	7.843E+00	1.007E+01	1.987E+00	2.564E+00	1.200E+00	5.913E-02	2.702E+00	2.502E+00
	3.000E+01	2.000E+00	1.800E+03	1.500E+01	1.216E+01	2.466E+00	1.972E+00	1.300E+00	6.891E-02	2.102E+00	1.945E+00
	5.000E+01	1.500E+00	3.750E+03	3.333E+01	1.554E+01	3.218E+00	1.457E+00	1.400E+00	7.934E-02	1.568E+00	1.463E+00
	7.000E+01	1.270E+00	6.223E+03	5.512E+01	1.839E+01	3.806E+00	1.215E+00	1.500E+00	9.041E-02	1.310E+00	1.238E+00
	1.000E+02	1.070E+00	9.070E+04	9.346E+01	2.204E+01	4.538E+00	1.017E+00	1.600E+00	1.021E-01	1.095E+00	1.055E+00
	2.000E+02	7.700E-01	3.080E+04	2.597E+02	3.135E+01	6.380E+00	7.537E-01	1.700E+00	1.144E-01	7.960E-01	8.060E-01
	3.000E+02	6.500E-01	5.850E+04	4.615E+02	3.882E+01	7.728E+00	6.495E-01	1.800E+00	1.272E-01	6.729E-01	7.030E-01
	5.000E+02	5.500E-01	1.375E+05	9.091E+02	5.161E+01	9.687E+00	5.529E-01	1.900E+00	1.406E-01	5.568E-01	6.003E-01
	7.000E+02	5.000E-01	2.450E+05	1.400E+03	6.257E+01	1.119E+01	5.046E-01	2.000E+00	1.545E-01	4.996E-01	5.442E-01
	1.000E+03	4.600E-01	4.600E+05	2.174E+03	7.719E+01	1.295E+01	4.634E-01	2.100E+00	1.690E-01	4.533E-01	4.924E-01
	2.000E+03	4.200E-01	1.680E+06	4.762E+03	1.189E+02	1.682E+01	4.049E-01	2.200E+00	1.839E-01	4.015E-01	4.151E-01
	3.000E+03	4.000E-01	3.600E+06	7.500E+03	1.533E+02	1.957E+01	3.803E-01	2.300E+00	1.993E-01	3.911E-01	3.889E-01
	5.000E+03	3.850E-01	9.625E+06	1.299E+04	2.127E+02	2.351E+01	3.563E-01	2.400E+00	2.152E-01	3.961E-01	3.818E-01
	7.000E+03	3.900E-01	1.911E+07	1.795E+04	2.674E+02	2.618E+01	3.439E-01	2.500E+00	2.315E-01	4.063E-01	3.914E-01

(continued)

**Table 4.1** (continued)

L&Sh	Re	$C_D$	$C_D Re^2$	$Re/C_D$	$d^* = (C_D Re^2)^{1/3}$	$u^* = (Re/C_D)^{1/3}$	Concha and Almendrala			H&L		B&Z
							$C_D$ sim	$d^*$ sim	$u^*$ sim	$C_D$ sim	$C_D$ sim	
1.000E+04	4.050E-01	4.050E+07	2.469E+04	3.434E+02	2.912E+01	3.330E-01	2.600E+00	2.482E-01	4.204E-01	4.090E-01		
2.000E+04	4.500E-01	1.800E+08	4.444E+04	5.646E+02	3.542E+01	3.170E-01	2.700E+00	2.653E-01	4.475E-01	4.456E-01		
3.000E+04	4.700E-01	4.230E+08	6.383E+04	7.507E+02	3.996E+01	3.101E-01	2.800E+00	2.829E-01	4.592E-01	4.619E-01		
5.000E+04	4.900E-01	1.225E+09	1.020E+05	1.070E+03	4.673E+01	3.031E-01	2.900E+00	3.008E-01	4.681E-01	4.759E-01		
7.000E+04	5.000E-01	2.450E+09	1.400E+05	1.348E+03	5.192E+01	2.995E-01	3.000E+00	3.190E-01	4.708E-01	4.818E-01		
1.000E+05	4.800E-01	4.800E+09	2.083E+05	1.687E+03	5.928E+01	2.963E-01	3.100E+00	3.376E-01	4.715E-01	4.861E-01		
2.000E+05	4.200E-01	1.680E+10	4.762E+05	2.561E+03	7.809E+01	2.915E-01	3.200E+00	3.566E-01	4.686E-01	4.904E-01		
3.000E+05	2.000E-01	1.800E+10	1.500E+06	2.621E+03	1.145E+02	2.893E-01	3.300E+00	3.758E-01	4.655E-01	4.915E-01		
5.000E+05	8.400E-02	2.100E+10	5.952E+06	2.759E+03	1.812E+02	2.872E-01	3.400E+00	3.954E-01	4.610E-01	4.921E-01		
7.000E+05	1.000E-01	4.900E+10	7.000E+06	3.659E+03	1.913E+02	2.861E-01	3.500E+00	4.152E-01	4.579E-01	4.922E-01		
1.000E+06	1.300E-01	1.300E+11	7.692E+06	5.066E+03	1.974E+02	2.851E-01	3.600E+00	4.353E-01	4.548E-01	4.921E-01		
3.000E+06	2.000E-01	1.800E+12	1.500E+07	1.216E+04	2.466E+02	2.829E-01	3.700E+00	4.557E-01	4.462E-01	4.916E-01		

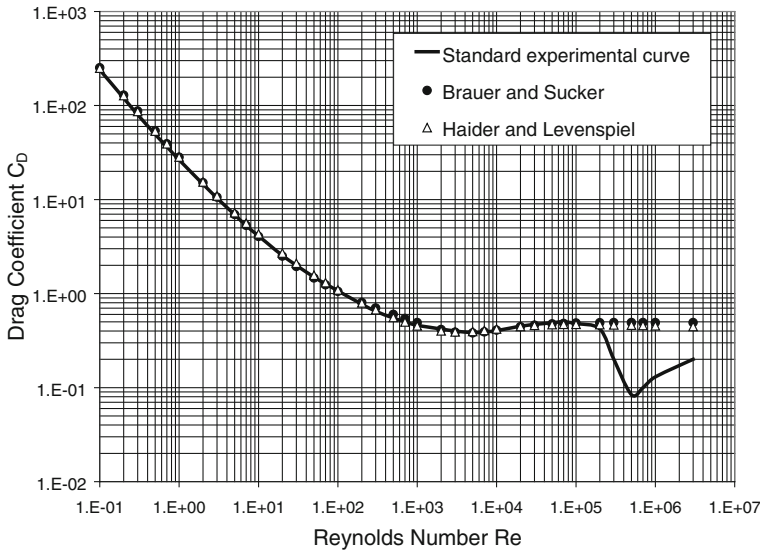


**Fig. 4.12** Comparison of the drag coefficient for a sphere, simulated by Brauer and Zucker (1976) and by Haider and Levenspiel (1998), and standard experimental points from Laple and Shepherd (1940)

Concha and Almendra (1979a) defined the characteristic parameters  $P$  and  $Q$  of the solid–liquid system:

$$P = \left( \frac{3}{4} \frac{\mu_f^2}{\Delta \rho \rho_f g} \right)^{1/3} \quad Q = \left( \frac{4 \Delta \rho \mu_f g}{3 \rho_f^2} \right)^{1/3} \quad (4.45)$$

so that Eq. (4.44) may be written in the form:

$$C_D Re_\infty^2 = \left( \frac{d}{P} \right)^3 = d^{*3} \quad \frac{Re_\infty}{C_D} = \left( \frac{u_\infty}{Q} \right)^3 \equiv u_\infty^{*3} \quad (4.46)$$

Expressions (4.46) define a dimensionless size  $d^*$  and a dimensionless velocity  $u^*$ , which are characteristics of a solid–liquid system:

$$d^* = \left( \frac{d}{P} \right) \quad u_\infty^* = \left( \frac{u_\infty}{Q} \right) \quad (4.47)$$

Since there is a direct relationship between the Drag Coefficient and the Reynolds Number, see for example Eqs. (4.37)–(4.39), there must be a relationship between the dimensionless groups  $C_D Re^2$  and  $Re/C_D$ . Table 4.1 gives that relationship.

Multiplying the two terms in Eq. (4.47), we can observe that the Reynolds number may be written in terms of the dimensionless size and dimensionless velocity:

$$Re_\infty = d^* u_\infty^* \quad (4.48)$$

Replacing (4.37) and (4.48) into (4.46) we obtain:

$$\begin{aligned} d^{*3} &= C_0 \left( 1 + \frac{\delta_0}{(u_\infty^* d^*)^{1/2}} \right)^2 (u_\infty^* d^*)^2 \\ u_\infty^* d^* + \delta_0 (u_\infty^* d^*)^{1/2} - \frac{d^{*3/2}}{C_0^{1/2}} &= 0 \end{aligned}$$

Solving these algebraic equations, explicit expressions are obtained for the dimensionless settling velocity  $u_\infty^*$  of a sphere of dimensionless size  $d^*$  and for the dimensionless sphere of diameter  $d^*$  settling a dimensionless velocity  $u_\infty^*$  (Concha and Almendra 1979a):

$$u_\infty^* = \frac{1}{4} \frac{\delta_0^2}{d^*} \left( \left( 1 + \frac{4}{C_0^{1/2} \delta_0^2} d^{*3/2} \right)^{1/2} - 1 \right)^2 \quad (4.49)$$

$$d^* = \frac{1}{4} C_0 u_\infty^{*2} \left( 1 + \left( 1 + \frac{4\delta_0}{C_0^{1/2} u_\infty^{*-3/2}} \right)^{1/2} \right)^2 \quad (4.50)$$

Equations (4.49) and (4.50) are known as *Concha and Almendra's equations* for a sphere. These two equations are general for spheres settling in a fluid at any Reynolds number. Introducing the values of  $C_0 = 0.284$  and  $\delta_0 = 9.06$ , the following final equations are obtained [In Concha and Amendra's paper (1979a),  $C_0 = 0.28$  was used].

$$u^* = \frac{20.52}{d^*} \left( \left( 1 + 0.0914 d^{*3/2} \right)^{1/2} - 1 \right)^2 \quad (4.51)$$

$$d^* = 0.071 u^{*2} \left( 1 + \left( 1 + 68.0 u^{*-3/2} \right)^{1/2} \right)^2 \quad (4.52)$$

**Problem 4.3** To calculate sedimentation velocities, it is necessary to know the sedimentation parameters  $P$  and  $Q$  that depend on the solid and fluid properties. Construct a table for these parameters as functions of the solid density. Assume that the fluid density is 1 g/cm<sup>3</sup> and its viscosity 0.01 g/cm s. Using the definition of  $P$  and  $Q$  from Eq. (4.45), Table 4.2 is obtained.

**Table 4.2** Parameters  $P$  and  $Q$  for several values of the solid density

$\rho_s$ (g/cm <sup>3</sup> )	$\rho_f$ (g/cm <sup>3</sup> )	$\mu_f$ (g/cm s)	$P$ (cm)	$Q$ (cm/s)	$\rho_s$ (g/cm <sup>3</sup> )	$\rho_f$ (g/cm <sup>3</sup> )	$\mu_f$ (g/cm s)	$P$ (cm)	$Q$ (cm/s)
1.10	1	0.0100	9.1470E-03	1.0933E+00	3.35	1	0.0100	3.1934E-03	3.1314E+00
1.15	1	0.0100	7.9906E-03	1.2515E+00	3.40	1	0.0100	3.1711E-03	3.1533E+00
1.20	1	0.0100	7.2600E-03	1.3774E+00	3.45	1	0.0100	3.1494E-03	3.1752E+00
1.25	1	0.0100	6.7396E-03	1.4838E+00	3.50	1	0.0100	3.1282E-03	3.1967E+00
1.30	1	0.0100	6.3422E-03	1.5767E+00	3.55	1	0.0100	3.1076E-03	3.2179E+00
1.35	1	0.0100	6.0245E-03	1.6599E+00	3.60	1	0.0100	3.0876E-03	3.2388E+00
1.40	1	0.0100	5.7622E-03	1.7354E+00	3.65	1	0.0100	3.0681E-03	3.2594E+00
1.45	1	0.0100	5.5404E-03	1.8049E+00	3.70	1	0.0100	3.0490E-03	3.2798E+00
1.50	1	0.0100	5.3492E-03	1.8694E+00	3.75	1	0.0100	3.0304E-03	3.2999E+00
1.55	1	0.0100	5.1819E-03	1.9298E+00	3.80	1	0.0100	3.0123E-03	3.3198E+00
1.60	1	0.0100	5.0338E-03	1.9866E+00	3.85	1	0.0100	2.9945E-03	3.3394E+00
1.65	1	0.0100	4.9013E-03	2.0403E+00	3.90	1	0.0100	2.9772E-03	3.3588E+00
1.70	1	0.0100	4.7817E-03	2.0913E+00	3.95	1	0.0100	2.9603E-03	3.3780E+00
1.75	1	0.0100	4.6730E-03	2.1400E+00	4.00	1	0.0100	2.9438E-03	3.3970E+00
1.80	1	0.0100	4.5735E-03	2.1865E+00	4.05	1	0.0100	2.9276E-03	3.4158E+00
1.85	1	0.0100	4.4820E-03	2.2311E+00	4.10	1	0.0100	2.9118E-03	3.4343E+00
1.90	1	0.0100	4.3974E-03	2.2741E+00	4.15	1	0.0100	2.8963E-03	3.4524E+00
1.95	1	0.0100	4.3189E-03	2.3154E+00	4.20	1	0.0100	2.8811E-03	3.4709E+00
2.00	1	0.0100	4.2457E-03	2.3553E+00	4.25	1	0.0100	2.8663E-03	3.4889E+00
2.05	1	0.0100	4.1772E-03	2.3940E+00	4.30	1	0.0100	2.8517E-03	3.5067E+00
2.10	1	0.0100	4.1129E-03	2.4314E+00	4.35	1	0.0100	2.8375E-03	3.5243E+00
2.15	1	0.0100	4.0524E-03	2.4677E+00	4.40	1	0.0100	2.8235E-03	3.5417E+00
2.20	1	0.0100	3.9953E-03	2.5029E+00	4.45	1	0.0100	2.8098E-03	3.5590E+00
2.25	1	0.0100	3.9413E-03	2.5372E+00	4.50	1	0.0100	2.7963E-03	3.5761E+00
2.30	1	0.0100	3.8901E-03	2.5706E+00	4.55	1	0.0100	2.7831E-03	3.5931E+00
2.35	1	0.0100	3.8415E-03	2.6032E+00	4.60	1	0.0100	2.7702E-03	3.6098E+00

(continued)

**Table 4.2** (continued)

$\rho_s$ (g/cm <sup>3</sup> )	$\rho_f$ (g/cm <sup>3</sup> )	$\mu_f$ (g/cm s)	P (cm)	Q (cm/s)	$\rho_s$ (g/cm <sup>3</sup> )	$\rho_f$ (g/cm <sup>3</sup> )	$\mu_f$ (g/cm s)	P (cm)	Q (cm/s)
2.40	1	0.0100	3.7952E-03	2.6349E+00	4.65	1	0.0100	2.7575E-03	3.6265E+00
2.45	1	0.0100	3.7511E-03	2.6659E+00	4.70	1	0.0100	2.7450E-03	3.6430E+00
2.50	1	0.0100	3.7089E-03	2.6962E+00	4.75	1	0.0100	2.7328E-03	3.6593E+00
2.55	1	0.0100	3.6686E-03	2.7258E+00	4.80	1	0.0100	2.7207E-03	3.6755E+00
2.60	1	0.0100	3.6300E-03	2.7548E+00	4.85	1	0.0100	2.7089E-03	3.6915E+00
2.65	1	0.0100	3.5929E-03	2.7832E+00	4.90	1	0.0100	2.6973E-03	3.7075E+00
2.70	1	0.0100	3.5574E-03	2.8111E+00	4.95	1	0.0100	2.6858E-03	3.7232E+00
2.75	1	0.0100	3.5232E-03	2.8384E+00	5.00	1	0.0100	2.6746E-03	3.7389E+00
2.80	1	0.0100	3.4902E-03	2.8651E+00	5.05	1	0.0100	2.6635E-03	3.7544E+00
2.85	1	0.0100	3.4585E-03	2.8914E+00	5.10	1	0.0100	2.6527E-03	3.7698E+00
2.90	1	0.0100	3.4279E-03	2.9172E+00	5.15	1	0.0100	2.6420E-03	3.7850E+00
2.95	1	0.0100	3.3983E-03	2.9426E+00	5.20	1	0.0100	2.6315E-03	3.8002E+00
3.00	1	0.0100	3.3698E-03	2.9676E+00	5.25	1	0.0100	2.6211E-03	3.8152E+00
3.05	1	0.0100	3.3422E-03	2.9921E+00	5.30	1	0.0100	2.6109E-03	3.8301E+00
3.10	1	0.0100	3.3154E-03	3.0162E+00	5.35	1	0.0100	2.6009E-03	3.8449E+00
3.15	1	0.0100	3.2895E-03	3.0400E+00	5.40	1	0.0100	2.5910E-03	3.8596E+00
3.20	1	0.0100	3.2644E-03	3.0633E+00	5.45	1	0.0100	2.5812E-03	3.8741E+00
3.25	1	0.0100	3.2400E-03	3.0864E+00	5.50	1	0.0100	2.5716E-03	3.8886E+00
3.30	1	0.0100	3.2164E-03	3.1091E+00	5.55	1	0.0100	2.5622E-03	3.9029E+00

**Problem 4.4** Calculate the settling velocity of quartz spheres with density of 2.65 g/cm<sup>3</sup> of the following diameters: 1, 10, 50, 100 and 500 µm, and 0.1, 0.5 and 1.0 cm in water at 20 °C. Use Eq. (4.51):

$$u_{\infty}^* = \frac{20.52}{d^*} \left( \left( 1 + 0.0914 d^{*3/2} \right)^{1/2} - 1 \right)^2, \quad \text{with } d^* = d/P \quad \text{and} \quad u_{\infty} = Q \times u_{\infty}^*$$

---

<i>Data</i>								
$\rho_s$ (g/cm <sup>3</sup> )=	2.65	2.65	2.65	2.65	2.65	2.65	2.65	2.65
$\rho_f$ (g/cm <sup>3</sup> )=	1	1	1	1	1	1	1	1
$\mu$ (poises)=	0.01	0.01	0.01	0.01	0.01	0.01	0.01	0.01
$d_p$ (cm)=	0.0001	0.001	0.005	0.01	0.05	0.1	0.5	1
P (cm)=	0.00359	0.00359	0.00359	0.00359	0.00359	0.00359	0.00359	0.00359
Q (cm/s)=	2.78320	2.78320	2.78320	2.78320	2.78320	2.78320	2.78320	2.78320
<i>Results</i>								
$d^*$ =	2.78E-02	2.78E-01	1.39E+00	2.78E+00	1.39E+01	2.78E+01	1.39E+02	2.78E+02
$u^*$ =	3.32E-05	3.30E-03	7.73E-02	2.76E-01	2.88E+00	5.77E+00	1.88E+01	2.84E+01
$u_{\infty}$ (cm/s) =	9.24E-05	9.18E-03	2.15E-01	7.68E-01	8.01E+00	1.61E+01	5.23E+01	7.90E+01
Re =	9.24E-07	9.18E-04	1.08E-01	7.68E-01	4.00E+01	1.61E+02	2.62E+03	7.90E+03

---

**Problem 4.5** Compare the simulated dimensionless velocity versus dimensionless diameter predicted by Concha and Almendra's equation with experimental data from Table 4.1.

Using Eq. (4.51), the values of column  $d^*_{\text{sim}}$  and  $u^*_{\text{sim}}$  are obtained. The plot of these data is shown in Fig. 4.13.

### Effect of temperatures on the settling velocity

To calculate the settling velocity of spheres at different temperatures, it is necessary to know the density and viscosity of the fluid involved at these temperatures. In the case of water and air, the following correlations can be used for the density and viscosity. Figures 4.14 and 4.15 show the correlations of densities and viscosities for air and water.

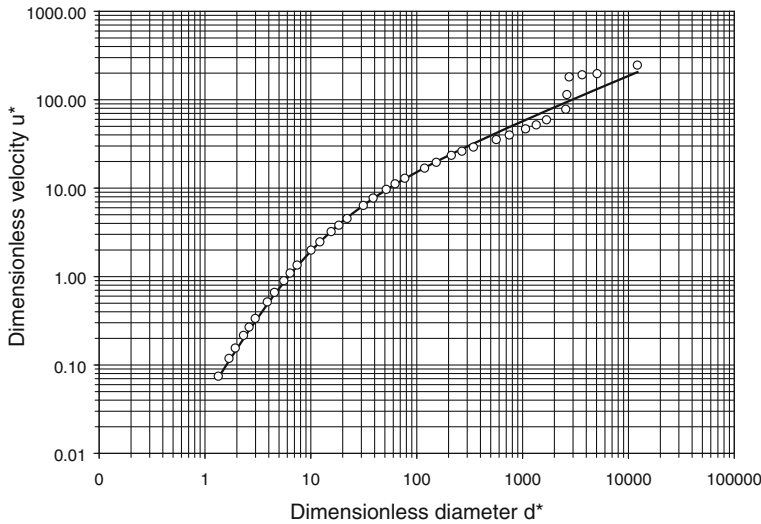


**Fig. 4.13** Dimensionless velocity versus dimensionless diameter for the sedimentation of spheres according to Eq. (4.51) of Concha and Almendra. Circles are standard data from Lapple and Shepherd (1940) in Table 4.1

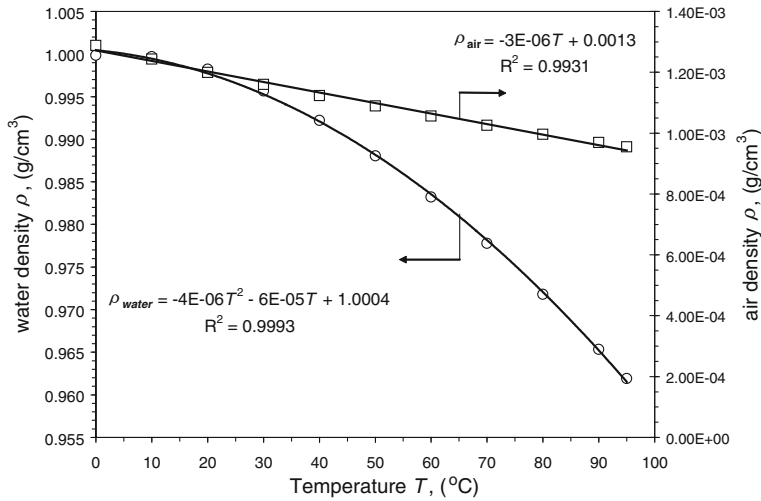


**Fig. 4.14** Water and air densities at several temperatures

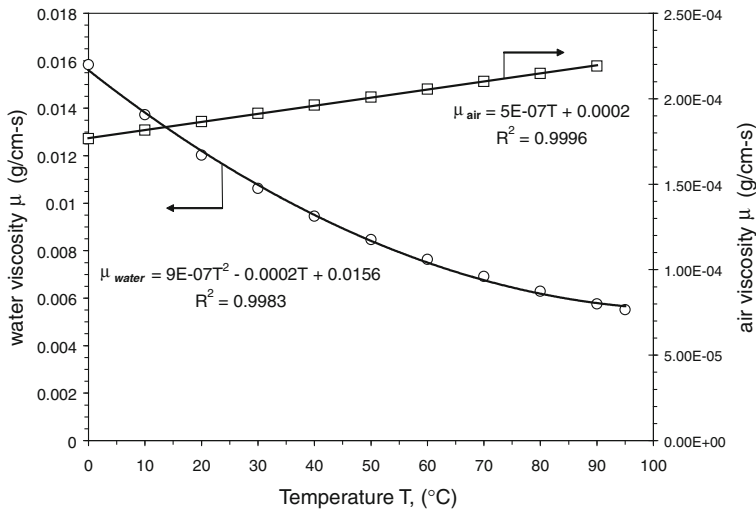


**Fig. 4.15** Water and air viscosities at several temperatures

### Density:

$$\rho_{water} = -4.0 \times 10^{-6}T^2 - 6.0 \times 10^{-5}T + 1.0004 \text{ g/cm}^3 \quad (4.53)$$

$$\rho_{air} = -3.0 \times 10^{-6}T + 1.3 \times 10^{-3} \text{ g/cm}^3 \quad (4.54)$$

### Viscosity:

$$\mu_{water} = 9.0 \times 10^{-7}T^2 - 2.0 \times 10^{-4}T + 1.56 \times 10^{-2} \text{ g/cm s} \quad (4.55)$$

$$\mu_{air} = 5.0 \times 10^{-7}T + 2.0 \times 10^{-4} \text{ g/cm s} \quad (4.56)$$

**Problem 4.6** Calculate the settling velocity of a quartz sphere of 300  $\mu\text{m}$  with density 2.65  $\text{g/cm}^3$  in water at 60 °C. From the correlations (4.55), (4.53) and from Eqs. (4.45) we obtain:

$$\rho_{water} = -4.0 \times 10^{-6} \times 20^2 - 6.0 \times 10^{-5} \times 20 + 1.0004 = 0.9976 \text{ g/cm}^3$$

$$\mu_{water} = 9 \times 10^{-7} \times 20^2 - 2 \times 10^{-4} \times 20 + 0.0156 = 0.01196$$

$$P = \left( \frac{3}{4} \frac{\mu_f^2}{\Delta \rho \rho_f g} \right)^{1/3} = 2.550 \times 10^{-3} \text{ cm}$$

$$Q = \left( \frac{4}{3} \frac{\Delta \rho \mu_f g}{\rho_f^2} \right)^{1/3} = 2.0534 \text{ cm/s}$$

$$d^* = \frac{300}{10,000 \times 2.5502 \times 10^{-3}} = 11.764$$

$$u^* = \frac{20.52}{d^*} \left( (1 + 0.0921 d^{*3/2})^{1/2} - 1 \right)^2 = 1.5017$$

$$u_\infty = u^* \times Q = 1.5017 \times 2.0534 = 3.0826 \text{ m/s}$$

#### 4.1.7 Sedimentation of a Suspension of Spheres

In a suspension, the spheres, surrounding a given sphere, hinder its motion as it settles. This hindrance is due to several effects. In the first place, when the particle changes its position, it can find the new site occupied by another particle, and will collide with it, thus changing its trajectory. The more concentrated the suspension is, the greater the chance of collision. The result is that hindrance is a function of concentration. On the other hand, the settling of each particle of the suspension produces a back flow of the fluid. This back flow will increase the drag on a given particle, retarding its sedimentation. Again, an increase in concentration will increase the hindrance. It is clear that in both cases, the hindrance depends on the fraction of volume occupied by the particles and not on their weight and therefore the appropriate parameter to measure hindrance is the volumetric concentration rather than the percentage by weight.

Several theoretical works have been devoted to study the interaction of particles in a suspension during sedimentation. These types of studies were discussed in Tory (1996). In a recent approach, Quispe et al. used the tools of lattice-gas and cellular automata to study the sedimentation of particles and the fluid flow through an ensemble of settling particles. They were able to obtain some important macroscopic properties of the suspensions. Unfortunately, none of these works has yielded a sufficiently general and simple relationship between the variables of the suspension and its settling velocity to be used for practical purposes.

Concha and Almendra (1979b) assumed that the same equations used for the drag coefficient and for the settling velocity of individual spherical particles are valid for a suspension of particles if parameters  $P$  and  $Q$  are replaced by

$P(\varphi)$  and  $Q(\varphi)$  depending on the volume fraction of solids. Write Eqs. (4.36) and (4.49) in the form:

$$C_D(\varphi) = C_0(\varphi) \left( 1 + \frac{\delta_0(\varphi)}{Re^{1/2}} \right)^2 \quad (4.57)$$

$$U^*(\varphi) = \frac{\delta_0^2}{D^*(\varphi)} \left( \left( 1 + \frac{1}{C_0^{1/2} \delta_0^2} D^{*3/2}(\varphi) \right)^{1/2} - 1 \right)^2 \quad (4.58)$$

where

$$D^* = \frac{d}{P(\varphi)} \quad \text{and} \quad U^* = \frac{u}{Q(\varphi)} \quad (4.59)$$

It is convenient to express the properties of a suspension, such as viscosity, as the product of the same property of the fluid with a function of concentration. Assume that  $P(\varphi)$  and  $Q(\varphi)$  can be related with  $P$  and  $Q$  in that form, then:

$$P(\varphi) = Pf_p(\varphi) \quad \text{and} \quad Q(\varphi) = Qf_q(\varphi) \quad (4.60)$$

Replacing (4.60) into (4.59), and using the definition (4.47) of  $d^*$  and  $u^*$ , results in:

$$D^* = \frac{d^*}{f_p(\varphi)} \quad \text{and} \quad U^*(\varphi) = \frac{u^*(\varphi)}{f_q(\varphi)} \quad (4.61)$$

With these definitions, Eq. (4.58) may be written in the form:

$$u^*(\varphi) = \frac{\delta_0^2}{d^* f_p(\varphi) f_q(\varphi)} \left( \left( 1 + \frac{1}{C_0^{1/2} \delta_0^2} f_p^{-3/2} d^{*3/2} \right)^{1/2} - 1 \right)^2 \quad (4.62)$$

Substituting the values of  $\delta_0 = 9.06$  and  $C_0 = 0.284$ , yields:

$$u^*(\varphi) = \frac{20.52}{d^*} f_p(\varphi) f_q(\varphi) \left( 1 + 0.0914 f_p^{-3/2}(\varphi) d^{*3/2} - 1 \right)^2 \quad (4.63)$$

This expression, known as *Concha and Almendra's equation for a suspension of spheres*, permits the calculation of the settling velocity of a sphere of any size and density when it forms part of a suspension with volume fraction  $\varphi$ . To perform the calculations, it is necessary to know the parameters  $f_p(\varphi)$  and  $f_q(\varphi)$ .

### Asymptotic expressions for the sedimentation velocity.

For small values of the Reynolds number,  $Re \rightarrow 0$ , the following expressions may be derived from (4.51) and (4.63), which reduce the settling equation to the expression indicated:

$$0.0921d^{*3/2}f_p^{-3/2} \ll 1 \Rightarrow u^*(\varphi) = 20.52 \left( \frac{0.0914}{2} \right)^2 d^{*2} f_p^{-2}(\varphi) f_q(\varphi)$$

$$0.0921d^{*3/2} \ll 1 \Rightarrow u_\infty^* = 20.52 \left( \frac{0.0914}{2} \right)^2 d^{*2}$$

In these expressions, the symbols  $u_\infty^*$  and  $u^*(\varphi)$  indicate the settling velocity of a particle in an infinite medium and the velocity of the same particle in a suspension. The quotient between these two terms is:

$$\text{For } Re_\infty \rightarrow 0 \quad \frac{u^*(\varphi)}{u_\infty^*} = f_p^{-2}(\varphi) f_q(\varphi) \quad (4.64)$$

With a similar deduction, we can write for high Reynolds numbers, Eq. (4.49) equation reference goes here (4.51) and (4.62) in the form:

$$0.0921d^{*3/2}f_p^{-3/2} \gg 1 \Rightarrow u^*(\varphi) = 20.52 \times 0.0914 \times d^{*1/2} f_p^{-1/2}(\varphi) f_q(\varphi)$$

$$0.0921d^{*3/2} \gg 1 \Rightarrow u_\infty^* = 20.52 \times 0.0914 \times d^{*1/2}$$

The quotient between these two equations is:

$$\text{for } Re_\infty \rightarrow \infty \quad \frac{u^*(\varphi)}{u_\infty^*} = f_p^{-1/2}(\varphi) f_q(\varphi) \quad (4.65)$$

To find functional forms for the functions  $f_p(\varphi)$  and  $f_q(\varphi)$  experimental values for the settling velocities  $u_\infty$  and  $u(\varphi)$  are needed.

### Functional form for $f_p(\varphi)$ and $f_q(\varphi)$

Several authors have presented expressions for the velocity ratio  $u/u_\infty$ . See Concha and Almendra (1979b). Richardson and Zaki (1954), made the most comprehensive and most cited work on the relative particle–fluid flow under gravity. We will use their data in this book.

Richardson and Zaki (1954) performed careful sedimentation and liquid fluidization tests with mono-sized spherical particles in a wide range of particles sizes, fluid densities and viscosities. The authors expressed their result in the form:

$$u(\varphi)/u_\infty = (1 - \varphi)^n \text{ for } Re \rightarrow 0 \quad \text{and} \quad u(\varphi)/u_\infty = (1 - \varphi)^m \text{ for } Re \rightarrow \infty \quad (4.66)$$

The characteristics of these particles and fluid are given in Table 4.3. Table 4.4 shows values for  $u(\varphi)/u_\infty$  obtained from their experimental results.

Instead of using the values of  $n$  presented by Richardson and Zaki (1954), we will optimize the values using all experimental data. From (4.64), (4.65) and (4.66), we can write

**Table 4.3** Experimental data of Richardson and Zaki (1954)

N°	d (cm)	$\rho_s$ (g/cm <sup>3</sup> )	$\mu_{fx102}$ (g/cms)	$\rho_f$ (g/cm <sup>3</sup> )	v <sub>st</sub> (cm/s)	Re <sub>oo</sub>	n + 1	n
P	0.0181	1.058	20.800	1.034	0.00206	0.000185	4.90	3.90
Q	0.0181	1.058	20.800	1.034	0.00206	0.000185	4.79	3.79
K	0.0096	2.923	62.000	1.208	0.01390	0.000216	4.75	3.75
L	0.0096	2.923	62.000	1.208	0.01390	0.000216	4.65	3.65
F	0.0358	1.058	20.800	1.034	0.00807	0.001430	4.92	3.92
G	0.0358	1.058	20.800	1.034	0.00807	0.001430	4.89	3.89
H	0.0096	2.923	20.800	1.034	0.04550	0.002180	4.76	3.76
I	0.0096	2.923	20.800	1.034	0.04550	0.002180	4.72	3.72
J	0.0096	2.923	20.800	1.034	0.04550	0.002180	4.69	3.69
R	0.0230	2.623	62.000	1.208	0.06590	0.002950	4.85	3.85
S	0.0230	2.623	62.000	1.208	0.06590	0.002950	4.80	3.80
T	0.0128	2.960	1.890	2.890	0.03307	0.064700	4.84	3.84
M	0.0128	2.960	1.890	2.890	0.03307	0.064700	4.72	3.72
C	0.0181	1.058	1.530	1.001	0.06400	0.078900	4.76	3.76
A	0.0181	1.058	1.530	1.001	0.06640	0.078900	4.90	3.90
B	0.0181	1.058	1.530	1.001	0.06640	0.078900	4.79	3.79
X	0.1029	2.976	112.900	1.221	0.89100	0.099500	5.30	4.30
Y	0.1029	2.976	112.900	1.221	0.89100	0.099500	5.20	4.20
D	0.0253	1.058	2.910	0.935	0.14750	0.120000	4.94	3.94
E	0.0253	1.058	2.910	0.935	0.14750	0.120000	4.90	3.90
N	0.0096	2.923	1.612	2.170	0.23400	0.030200	4.74	3.74
O	0.0096	2.923	1.612	2.170	0.23400	0.030200	4.65	3.65
2	0.0253	2.78	6.075	1.135	0.82700	0.391000	4.65	3.65
5	0.0253	1.06	1.000	1.000	0.19400	0.490000	4.53	3.53
8	0.0230	2.623	1.890	2.890	0.34900	1.227000	4.450	3.450
9	0.0230	2.623	1.890	2.890	0.34900	1.227000	4.520	3.520
12	0.0230	2.623	1.890	2.890	0.34900	1.227000	4.140	3.140
10	0.0230	2.623	1.612	2.170	0.65250	2.021000	4.300	3.300
11	0.0230	2.623	1.612	2.170	0.65250	2.021000	4.350	3.350
13	0.0230	2.623	1.612	2.170	0.65250	2.021000	4.240	3.240
6	0.0510	2.745	6.075	1.135	2.89000	2.745000	4.22	3.22
14	0.1029	2.976	10.960	1.153	6.03000	6.530000	4.300	3.300
15	0.1029	2.976	10.960	1.153	6.03000	6.530000	4.070	3.070
16	0.1029	2.976	10.960	1.153	6.03000	6.530000	4.000	3.000
4	0.0253	2.78	1.000	1.000	3.55000	8.971000	3.59	2.59
3	0.1029	10.6	15.010	0.875	19.60000	11.750000	3.72	2.72
1	0.1029	2.976	1.890	2.890	1.16000	18.180000	3.800	2.800
	0.1029	2.976	1.890	2.890	1.16000	18.180000	3.640	2.640
	0.1029	2.976	1.890	2.890	1.16000	18.180000	3.860	2.860
	0.1029	2.976	1.839	2.745	2.48000	38.260000	3.340	2.340
	0.1029	2.976	1.839	2.745	2.48000	38.260000	3.560	2.560

(continued)

**Table 4.3** (continued)

N°	d (cm)	$\rho_s$ (g/cm <sup>3</sup> )	$\mu_{fx102}$ (g/cms)	$\rho_f$ (g/cm <sup>3</sup> )	v <sub>st</sub> (cm/s)	Re <sub>oo</sub>	n + 1	n
0.1029	2.976	1.839	2.745	2.48000	38.260000	3.500	2.500	
0.0510	2.745	1.000	1.000	8.10000	41.720000	3.11	2.11	
0.1029	2.745	1.000	1.0	7.35000	14.450000	3.78	2.78	
0.1029	2.745	1.000	1.000	7.35000	14.450000	3.78	2.78	
0.4200	2.89	15.010	0.875	31.90000	78.250000	3.34	2.34	
0.1029	10.6	3.810	0.818	36.15000	79.800000	3.08	2.08	
0.2466	11.25	15.010	0.875	58.10000	80.350000	3.39	2.39	
0.3175	7.73	15.010	0.875	54.70000	101.200000	3.17	2.17	
0.4200	2.89	6.075	1.135	34.05000	267.000000	2.58	1.58	
0.1029	10.6	1.000	1.000	47.50000	488.700000	2.43	1.43	
0.4200	2.89	1.000	1.000	48.60000	2,041.000000	2.33	1.33	
0.3175	7.73	1.000	1.000	79.70000	2,530.000000	2.36	1.36	
0.6350	7.74	1.000	1.000	112.70000	7,150.000000	2.38	1.38	

$$\begin{aligned} f_p^{-2}(\varphi) f_q(\varphi) &= (1 - \varphi)^n \\ f_p^{-1/2}(\varphi) f_q(\varphi) &= (1 - \varphi)^m \end{aligned} \quad (4.67)$$

and, by solving this algebraic set, we obtain:

$$f_p = (1 - \varphi)^{(2/3)(m-n)} \quad \text{and} \quad f_q = (1 - \varphi)^{(1/3)(4m-n)} \quad (4.68)$$

Using Eq. (4.62) and the calculated values in Table 4.5 and Fig. 4.16. The best values for  $m$  and  $n$ , were  $n = 3.90$  and  $m = 0.85$ .

Then,

$$f_p(\varphi) = (1 - \varphi)^{-2.033}, \quad f_q(\varphi) = (1 - \varphi)^{-0.167} \quad (4.69)$$

A plot of Eq. (4.69) is given in Fig. 4.16.

Table 4.4 gives the data and Fig. 4.17 shows a plot of the dimensionless settling velocity versus Reynolds number for spheres, according to the experimental data of Richardson and Zaki (1954) and the simulation of Concha and Almendra (1979a, b) with Eqs. (4.62) and (4.69).

If all data of Table 4.4 are plotted in the form  $U^*$  versus  $D^*$  with the definitions (4.61), Fig. 4.18 is obtained.

On the other hand, Fig. 4.19 shows the settling velocity  $u^*$  versus  $d^*$  for suspensions of spheres in water at 20 °C for different values of the concentration  $\varphi$ . This figure can be used to visualize the state of flow of particulate systems.

In Chap. 5 of this textbook, Eq. (5.6), we will see that the volume average velocity, also known as *spatial velocity* or *percolation velocity*, is given by:

$$q = v_s - (1 - \varphi)v_r \quad (4.70)$$

**Table 4.4** V values of  $u/u_\infty$  from the experimental results of Richardson and Zaki (1954)

$Re_{00}$	0.000	0.010	0.050	0.100	0.150	0.200	0.300	0.400	0.500	0.585
0.00019	0.0021	0.96156	0.81869	0.66305	0.53056	0.41184	0.24882	0.13639	0.06699	0.03239
0.00019	0.0021	0.96263	0.82333	0.67078	0.54013	0.42925	0.25877	0.14428	0.07229	0.03568
0.00026	0.0139	0.96301	0.82502	0.67361	0.54365	0.43310	0.26249	0.14725	0.07433	0.03696
0.00026	0.0139	0.96398	0.82926	0.68075	0.55256	0.44287	0.27202	0.15497	0.07966	0.04035
0.00144	0.0081	0.96137	0.81786	0.66165	0.52884	0.41698	0.24705	0.13501	0.06606	0.03182
0.00144	0.0081	0.96166	0.81911	0.66375	0.53142	0.41978	0.24971	0.13709	0.06745	0.03267
0.00217	0.0455	0.96292	0.82460	0.67290	0.54277	0.43213	0.26156	0.14650	0.07381	0.03663
0.00217	0.0455	0.96330	0.82629	0.67574	0.54631	0.43601	0.26532	0.14953	0.07589	0.03794
0.00217	0.0455	0.96359	0.82756	0.67788	0.54898	0.43894	0.26817	0.15184	0.07748	0.03896
0.00295	0.0659	0.96205	0.82080	0.66655	0.53489	0.42254	0.25330	0.13992	0.06935	0.03384
0.00295	0.0659	0.96253	0.82290	0.67007	0.53925	0.42829	0.25785	0.14354	0.07179	0.03537
0.06473	0.0331	0.96214	0.82122	0.66725	0.53576	0.42449	0.25420	0.14064	0.06983	0.03414
0.06473	0.0331	0.96330	0.82629	0.67574	0.54631	0.43601	0.26532	0.14953	0.07589	0.03794
0.07579	0.0640	0.96292	0.82460	0.67290	0.54277	0.43213	0.26156	0.14650	0.07381	0.03663
0.07863	0.0664	0.96156	0.81869	0.66305	0.53056	0.41184	0.24882	0.13639	0.06699	0.03239
0.07863	0.0664	0.96263	0.82333	0.67078	0.54013	0.42925	0.25877	0.14428	0.07229	0.03568
0.09916	0.8910	0.95770	0.80207	0.63569	0.49717	0.38308	0.21574	0.11119	0.05077	0.02278
0.09916	0.8910	0.95867	0.80619	0.64242	0.50531	0.39172	0.22357	0.11701	0.05441	0.02488
0.11990	0.1475	0.96118	0.81702	0.66026	0.52712	0.41512	0.24529	0.13563	0.06515	0.03127
0.11990	0.1475	0.96156	0.81869	0.66305	0.53056	0.41684	0.24882	0.13639	0.06699	0.03239
0.30240	0.2340	0.96311	0.82544	0.67432	0.54454	0.43407	0.26343	0.14801	0.07484	0.03728
0.30240	0.2340	0.96398	0.82926	0.68075	0.55256	0.44287	0.27202	0.15497	0.07966	0.04035
0.39091	0.8270	0.96398	0.82926	0.68075	0.55256	0.44287	0.27202	0.15497	0.07966	0.04035
0.49082	0.1940	0.96514	0.83438	0.68941	0.56344	0.45489	0.28392	0.16477	0.08657	0.04484

(continued)

**Table 4.4** (continued)

$Re_{90}$	$u/u_\infty$	0.000	0.010	0.050	0.100	0.150	0.200	0.300	0.400	0.500	0.585
1.22741	0.3490	0.96592	0.83781	0.69524	0.57081	0.46308	0.29214	0.17164	0.09151	0.04811	
1.22741	0.3490	0.96524	0.83481	0.69013	0.56436	0.45591	0.28493	0.16561	0.08717	0.04524	
1.22741	0.3490	0.96893	0.85124	0.71833	0.60031	0.49625	0.32629	0.20109	0.11344	0.06319	
2.02024	0.6525	0.96738	0.84428	0.70632	0.58490	0.47885	0.30819	0.18531	0.10153	0.05490	
2.02024	0.6525	0.96689	0.84212	0.70261	0.58017	0.47353	0.30275	0.18664	0.09807	0.05254	
2.02024	0.6525	0.96796	0.84689	0.71080	0.59063	0.48530	0.31486	0.19108	0.10584	0.05787	
2.75371	2.8900	0.96816	0.84775	0.71230	0.59256	0.48747	0.31711	0.19304	0.10732	0.05890	
6.52757	6.0300	0.96738	0.84428	0.70632	0.58490	0.47885	0.30819	0.18531	0.10153	0.05490	
6.52757	6.0300	0.96962	0.84340	0.72364	0.60718	0.50406	0.33454	0.20841	0.11908	0.06721	
6.52757	6.0300	0.97030	0.85738	0.72900	0.61413	0.51200	0.34300	0.21600	0.12500	0.07147	
8.98150	3.5500	0.97431	0.87560	0.76118	0.65644	0.56105	0.39701	0.26632	0.16609	0.10250	
11.7571	1.9600	0.97303	0.86978	0.75083	0.64272	0.54501	0.37902	0.24921	0.15177	0.09143	
18.2520	1.1600	0.97225	0.86622	0.74452	0.63441	0.53537	0.36836	0.23923	0.14359	0.08522	
18.2520	1.1600	0.97382	0.87335	0.75718	0.65113	0.55483	0.38999	0.25961	0.16043	0.09810	
18.2520	1.1600	0.97167	0.86355	0.73983	0.62826	0.52825	0.36056	0.23201	0.13774	0.08084	
38.0915	2.4800	0.97676	0.88690	0.78150	0.68366	0.59324	0.43404	0.30260	0.19751	0.12771	
38.0915	2.4800	0.97460	0.87695	0.76359	0.65965	0.56482	0.40128	0.27044	0.16958	0.10525	
38.0915	2.4800	0.97519	0.87965	0.76843	0.66611	0.57243	0.40996	0.27885	0.17678	0.11095	
41.3100	8.1000	0.97902	0.89742	0.80067	0.70970	0.62448	0.47115	0.34033	0.23165	0.15634	
75.6315	7.3500	0.97245	0.86710	0.74610	0.63648	0.53776	0.37100	0.24169	0.14559	0.08673	
75.6315	7.3500	0.97245	0.86710	0.74610	0.63648	0.53776	0.37100	0.24169	0.14559	0.08673	
78.1029	31.900	0.97676	0.88690	0.78150	0.68366	0.59324	0.43404	0.30260	0.19751	0.12771	
79.8642	36.150	0.97931	0.89880	0.80320	0.71317	0.62868	0.47622	0.34558	0.23651	0.16052	
83.5212	58.100	0.97627	0.88463	0.77739	0.67813	0.58666	0.42637	0.29497	0.19078	0.12222	

(continued)

**Table 4.4** (continued)

$Re_{90}$	$u/u_\infty$	0.000	0.010	0.050	0.100	0.150	0.200	0.300	0.400	0.500	0.585
101.241	54.700	0.97843	0.89466	0.79562	0.70281	0.61618	0.46117	0.33006	0.22221	0.14831	
267.187	34.050	0.98425	0.92215	0.84665	0.77354	0.70288	0.56919	0.44615	0.33448	0.24918	
488.775	47.500	0.98573	0.92928	0.86014	0.79263	0.72681	0.60047	0.48168	0.37113	0.28432	
2,041.20	48.600	0.98672	0.93405	0.86925	0.80561	0.74321	0.62227	0.50692	0.39777	0.31046	
2,530.48	79.700	0.98642	0.93262	0.86650	0.80170	0.73825	0.61565	0.49921	0.38958	0.30237	
7,156.45	112.70	0.98623	0.93166	0.86468	0.79909	0.73496	0.61127	0.49414	0.38422	0.29710	

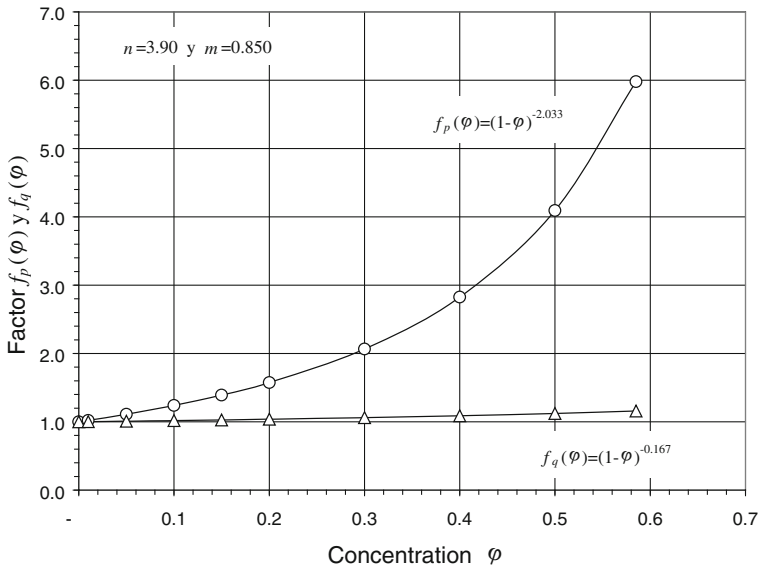


**Fig. 4.16** Parameters  $f_p(\varphi)$  and  $f_q(\varphi)$  from data by Richardson and Zaki

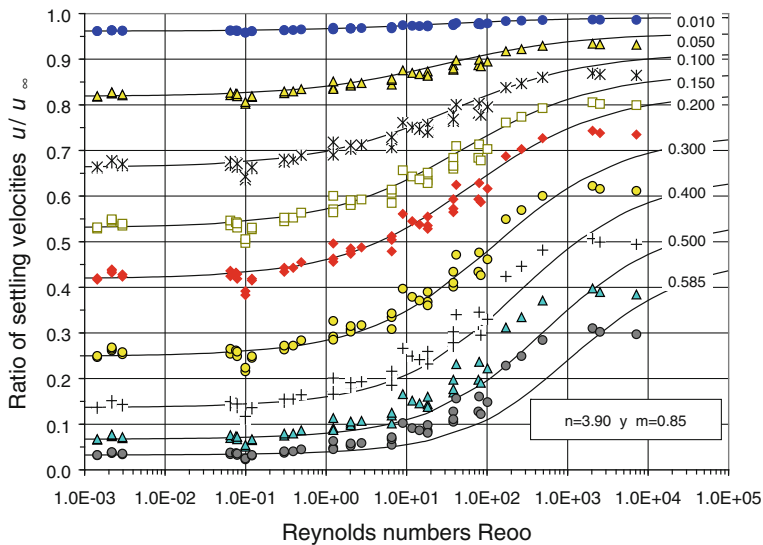


**Fig. 4.17** Dimensionless settling velocities versus Reynolds number, together with data obtained from Richardson and Zaki (1954) experimental results

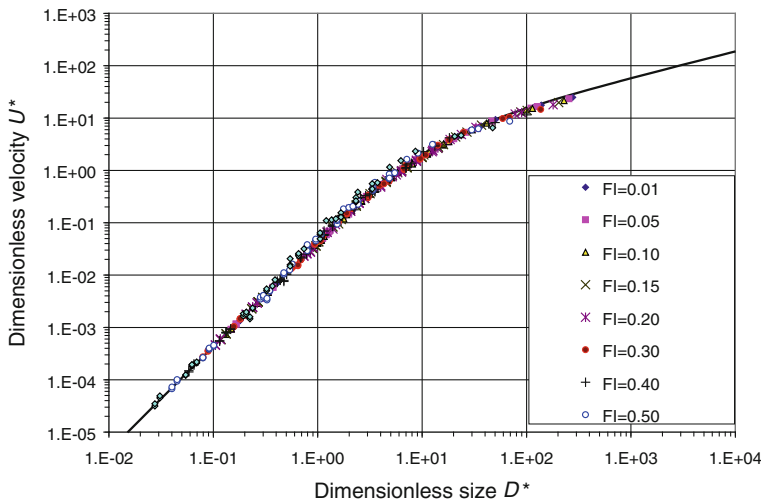


**Fig. 4.18** Dimensionless velocity  $U^*$  for suspensions of spheres of any size and density versus the dimensionless diameter  $D^*$ , with experimental data of Richardson and Zaki (1954)

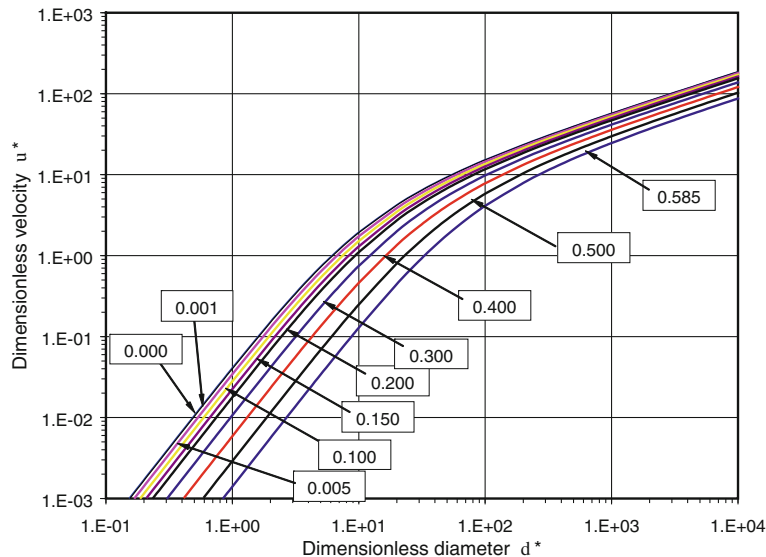


**Fig. 4.19** Simulation of the dimensionless velocity  $u^*$  versus the dimensionless size  $d^*$  for spherical particles settling in a suspension in water at  $20^\circ\text{C}$  with the volume fraction of solids a parameter

where  $q$ ,  $v_s$  and  $v_r$  are the spatial velocity, the solid component velocity and the relative solid–fluid velocity. Figure 4.17 divides the  $u^* \times d^*$  plane into three regions: a *porous bed*, between the  $d^*$  axis and the line of constant concentration  $\varphi = 0.585$  [Barnea and Mednick (1975) demonstrated that this concentration corresponds to the minimum fluidization velocity], a second region of a fluidized bed between  $0.585 \leq \varphi \leq 0$  and a third region of *hydraulic or pneumatic transport*, for values of velocities above concentration  $\varphi = 0$ .

### Drag Coefficient for a suspension of spheres

From Eqs. (4.49) and (4.62) we deduce that:

$$\begin{aligned}\tilde{\delta}_0^2 &= \delta_0^2 f_p(\varphi) f_q(\varphi) \\ \tilde{C}_0^{1/2} \tilde{\delta}_0^2 &= C_0^{1/2} \delta_0^2 f_p^{3/2}(\varphi)\end{aligned}$$

therefore, the parameters of the Drag Coefficient are:

$$\tilde{C}_0 = C_0 f_p(\varphi) f_q^{-2}(\varphi) \quad (4.71)$$

$$\tilde{\delta}_0 = \delta_0 f_p^{1/2}(\varphi) f_q^{1/2}(\varphi) \quad (4.72)$$

and the Drag Coefficient of the sphere can be written in the form:

$$C_D = C_0 f_p(\varphi) f_q^{-2}(\varphi) \left( 1 + \frac{\delta_0 f_p^{1/2}(\varphi) f_q^{1/2}(\varphi)}{\text{Re}^{1/2}} \right)^2 \quad (4.73)$$

Using the values for  $f_p(\varphi)$  and  $f_q(\varphi)$  from (4.69), we obtain finally:

$$C_D = 0.284(1 - \varphi)^{-2.01} \left( 1 + \frac{9.08(1 - \varphi)^{-1.83}}{\text{Re}^{1/2}} \right)^2 \quad (4.74)$$

**Problem 4.7** Consider a porous bed formed by spherical particles of dimensionless diameter  $d^* = 10$ . A fluid percolates through the bed at a dimensionless velocity  $u^* = 0.001$ . If the velocity is increased, establish the range of velocities at which the three regimes are present.

Drawing a vertical line in the plot of dimensionless velocity versus dimensionless size, Fig. 4.20, for  $d^* = 10$ , see lines in red in the next figure, we find that the system of particles forms a porous bed until the dimensionless velocity  $u^* \approx 0.130$ , which is the dimensionless minimum fluidization velocity. Fluidization exists for the range of dimensionless velocities  $0.13 \leq u^* \leq 2.00$ . For greater velocities, particles are transported.

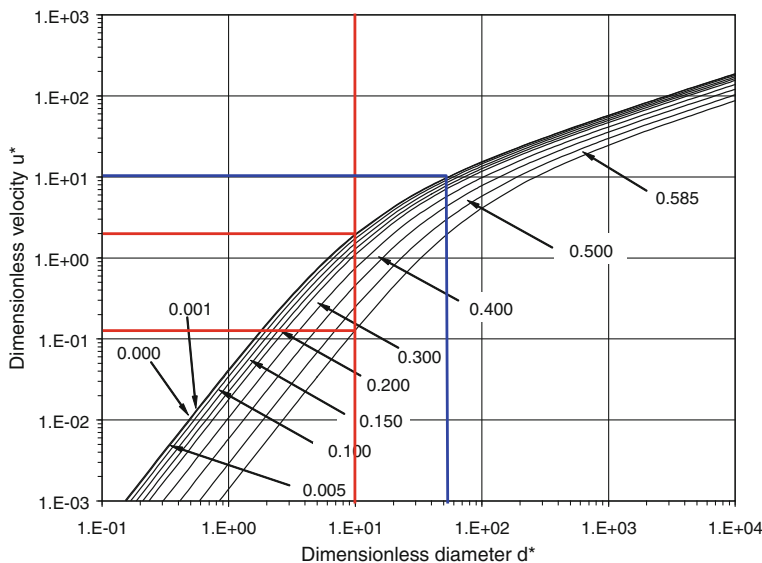


**Fig. 4.20** Plot of dimensionless diameter versus dimensionless size for spheres of Problem 4.7

**Problem 4.8** Determine the sedimentation velocity of a sphere, 150  $\mu\text{m}$  in diameter and  $2.65 \text{ g/cm}^3$  in density at  $15^\circ\text{C}$ , forming a suspension of 40 % of solid by weight.

The volume fraction of solids is:

$$\varphi = \frac{0.9989 \times 40}{2.65 \times (100 - 40) + 0.9989 \times 40} = 0.201$$

Parameters for the solid–fluid system:

$$\rho_{\text{water}} = 0.9986, \mu_{\text{water}} = 0.01280, P = 2.66 \times 10^{-3}, Q = 2.099$$

$$f_p(0.201) = 1.5761, f_q(0.201) = 1.0381$$

$$d^* = 5.622$$

$$u^* = \frac{20.52}{d^*} f_p(\varphi) f_q(\varphi) \left( \left( 1 + 0.0921 f_p^{3/2} d^{*3/2} \right)^{1/2} - 1 \right)^2 = 1.863$$

$$u = 1.863 \times 2.0987 = 3.910 \text{ cm/s} (\mathbf{u} = -3.91 \mathbf{k} \text{ cm/s})$$

**Problem 4.9** Determine the fluidization velocity of a 40 % by weight suspension of mono-sized quartz spherical particles, 150  $\mu\text{m}$  in diameter and  $2.65 \text{ g/cm}^3$  in density at  $15^\circ\text{C}$ . Calculate at which volume average velocity these particles begin to be transported.

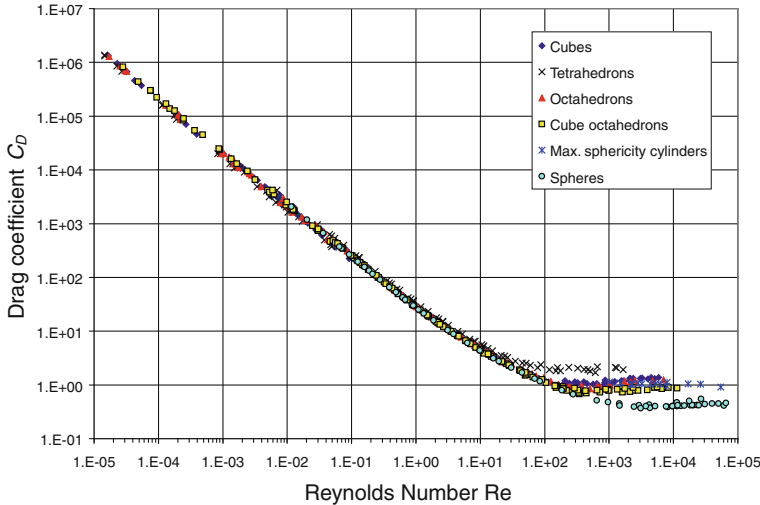


**Fig. 4.21** Plot of the drag coefficient versus the Reynolds number for the settling of isometric particles according to Pettyjohn and Christiansen (1948) and Barker (1951)

From the previous problem, we know that the sedimentation velocity for the same suspension is  $u = -3.91 \text{ cm/s}$ . The volume average velocity is given by  $q = v_s - (1 - \varphi)u$ , and since for fluidization  $v_s = 0$ ,  $q = -(1 - \varphi)u$

$$q = (1 - 0.201) \times 3.91 = 3.13 \text{ cm/s}.$$

The dimensionless particle size is  $d^* = 5.62$ . A straight line for this value in blue in Fig. 4.21 gives a transport velocity of  $u^* = 10$ , which corresponds to a velocity  $u = -10 \times 3.91 = -39.1 \text{ cm/s}$ . Then:

$$u = -39.1 \text{ cm/s}, q = -(1 - 0) \times -39.1 = 39.1 \text{ cm/s}.$$

#### 4.1.8 Sedimentation of Isometric Particles

The behavior of non-spherical particles is different than that of spherical particles during sedimentation. While spherical particles fall in a vertical trajectory, non-spherical particles rotate, vibrate and follow spiral trajectories. Several authors have studied the sedimentation of *isometric particles*, which have a high degree of symmetry with three equal mutually perpendicular symmetry axes, such as the tetrahedron, octahedron and dodecahedron. Wadell (1932, 1934), Pettyjohn and Christiansen (1948) and Christiansen and Barker (1965) show that isometric particles follow vertical trajectories at low Reynolds numbers, but rotate and vibrate

and show helicoidally trajectories for Reynolds numbers between 300 and 150,000. Figure 4.18 shows the drag coefficient versus Reynolds number for these particles.

Pettyjohn and Christiansen (1948) demonstrate that velocities in Stokes flow for isometric particles may be described with the following expression:

$$\frac{u_p}{u_e} = 0.843 \log\left(\frac{\psi}{0.065}\right) \quad \text{with} \quad u_e = \frac{\Delta\rho d_e^2 g}{18\mu_f} \quad (4.75)$$

where  $d_e$  is the volume equivalent diameter, that is, the diameter of a sphere with the same volume as the particle, and  $u_e$  is its settling velocity.

In the range of  $2,000 \leq Re \leq 17,000$ , the same authors derived the following equation for the settling velocity:

$$u_e = \frac{4}{3} \frac{\Delta\rho d_e g}{\rho_f C_D}, \quad (4.76)$$

with the drag coefficient  $C_D$  given by:  $C_D = (5.31 - 4.88\psi)/(1.433 \times 0.43)$ . The value of 1.433 in the denominator of this equation is a factor that takes the theoretical value of  $C_D = 0.3$  (see Fig. 4.11) to the average experimental value  $C_D = 0.43$  (see Fig. 4.19).

As we have already said, for  $Re > 300$ , the particles begin to rotate and oscillate, which depends on the particle density. To take into account these behavior, Barker (1951) introduced the particle to fluid density ratio as a new variable in the form:

$$C_D(\psi, \lambda) = \lambda^{1/18} \frac{(5.31 - 4.88\psi)}{0.62}, \quad (4.77)$$

where  $\lambda$  is the quotient between the solid and fluid densities  $\lambda = \rho_p/\rho_f$ .

Data from Pettyjohn and Christiansen (1948) and from Barker (1951) are plotted in Fig. 4.21. Figure 4.22 gives details of the higher end of the Reynolds range.

### Drag coefficient and sedimentation velocity

Results obtained for spherical particles (Concha and Almendra 1979a, b), may be used to develop functions for the drag coefficient and sedimentation velocity of isometric particles.

Assume that Eqs. (4.73) and (4.62) valid for isometric particles, with values of  $C_0$  and  $\delta_0$  as functions of the sphericity  $\psi$  and of the density quotient  $\lambda$  (Concha and Barrientos 1986):

$$C_D(\psi, \lambda) = \tilde{C}_0(\psi, \lambda) \left(1 + \frac{\delta_0(\psi, \lambda)}{Re^{1/2}}\right)^2 \quad (4.78)$$

$$u_p^* = \frac{1}{4} \frac{\tilde{\delta}_0^2(\psi, \lambda)}{d^*} \left( \left(1 + \frac{4}{\tilde{C}_0^{1/2}(\psi, \lambda) \tilde{\delta}_0^2(\psi, \lambda)} d^{*3/2}\right)^{1/2} - 1 \right)^2 \quad (4.79)$$

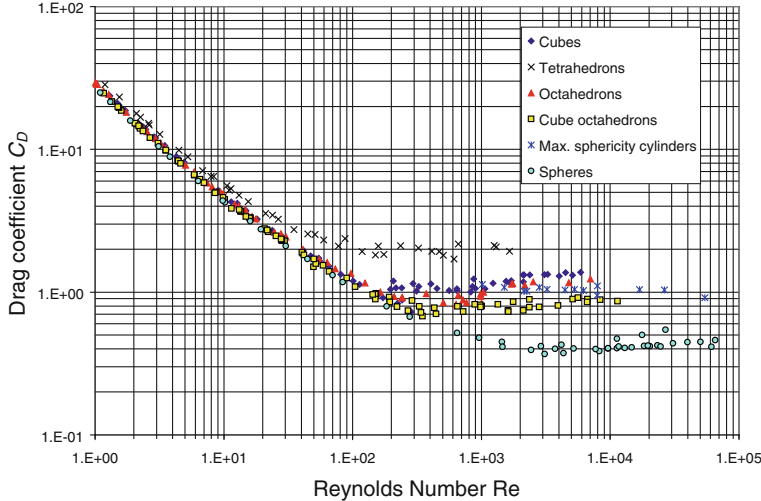


**Fig. 4.22** Details for Fig. 4.18 at the high end of the Reynolds range (Pettyjohn and Christiansen 1948; Barker 1951)

where the Reynolds number is defined using the volume equivalent diameter. Assume also that:

$$\tilde{C}_0(\psi, \lambda) = C_0 f_A(\psi) f_C(\lambda) \quad (4.80)$$

$$\tilde{\delta}_0(\psi, \lambda) = \delta_0 f_B(\psi) f_D(\lambda) \quad (4.81)$$

where  $C_0$  and  $\delta_0$  are the same parameters of a sphere.

We have already demonstrated that for a sphere (volume equivalent sphere in this case) at a low Reynolds number,  $Re \rightarrow 0$ , the dimensionless velocity can be approximated by Eq. (4.64).

Assume that we can approximate the velocity of isometric particles at low Reynolds numbers,  $Re \rightarrow 0$ , in the same way as for spherical particles. Then:

$$u_e^* = \frac{d_e^{*2}}{C_0 \delta_0^2} \quad \text{and} \quad u_p^* = \frac{d_e^{*2}}{\tilde{C}_0(\psi, \lambda) \delta_0^2(\psi, \lambda)} \quad (4.82)$$

Taking the quotient of these terms and substituting (4.80) and (4.81), results in:

$$Re \rightarrow 0, \quad \frac{u_e^*}{u_p^*} \equiv \frac{u_e}{u_p} = f_A(\psi) f_B^2(\psi) f_C(\lambda) f_D^2(\lambda) \quad (4.83)$$

On the other hand, for  $Re \rightarrow \infty$ :

$$\frac{C_D(\psi, \lambda)}{C_D} = \frac{\tilde{C}_0(\psi, \lambda)}{C_0} \quad \text{and} \quad \frac{C_D(\psi, \lambda)}{C_D} = f_A(\psi) f_C(\lambda) \quad (4.84)$$

To determine the functions  $f_A, f_B, f_C$  and  $f_D$  we will use the correlations presented by Pettyjohn and Christiansen (4.75) and (4.77), and by Barker (1951). From (4.83) and (4.75) we can write:

$$f_A(\psi)f_B^2(\psi)f_C(\lambda)f_D^2(\lambda) = \left\{ 0.843 \log \frac{\psi}{0.065} \right\}^{-1} \quad (4.85)$$

$$f_A(\psi)f_C(\lambda) = \lambda^{1/18} \frac{5.31 - 4.88\psi}{0.62} \quad (4.86)$$

From (4.77) and (4.86) we deduce that:

$$f_A(\psi) = \frac{5.31 - 4.88\psi}{0.62} \quad f_C(\lambda) = \lambda^{1/18}. \quad (4.87)$$

Since in the Stokes regime the density does not influence the flow, Eq. (4.85) implies that (Fig. 4.23):

$$f_C(\lambda)f_D^2(\lambda) = 1 \Rightarrow f_D(\lambda) = \lambda^{-1/36} \quad (4.88)$$

Therefore:

$$f_B(\psi) = \left\{ \frac{5.31 - 4.88\psi}{0.62} \times 0.843 \log \frac{\psi}{0.065} \right\}^{-1/2} \quad (4.89)$$

**Problem 4.10** Using Concha and Barrientos (1986) model for isometric particles, determine the values of the dimensionless velocity versus the dimensionless size for particles with sphericities 0.4, 0.5, 0.6, 0.7, 0.8, 0.9 and 1.0 for values of  $d^*$  from 0.01 to 100.000.

The result is shown in Fig. 4.24.

Haider and Levenspiel (1998) give an alternative equation for the Drag Coefficient and the settling velocity of isometric particles based on their equation for spherical particles:

$$C_D(\psi) = \frac{24}{Re} (1 + (8.1716 \times \exp(-4.0655\psi))) \text{Re}^{(0.0964+0.5565\psi)} + \frac{73.69 \text{Re} \times \exp(-5.0740\psi)}{\text{Re} + 5.378 \times \exp(6.2122\psi)} \quad (4.90)$$

$$u^* = \left( \frac{18}{d^{*2}} + \frac{3.1131 - 2.3252\psi}{d^{*0.5}} \right)^{-1}, \quad \text{for } 0.5 \leq \psi \leq 1 \quad (4.91)$$

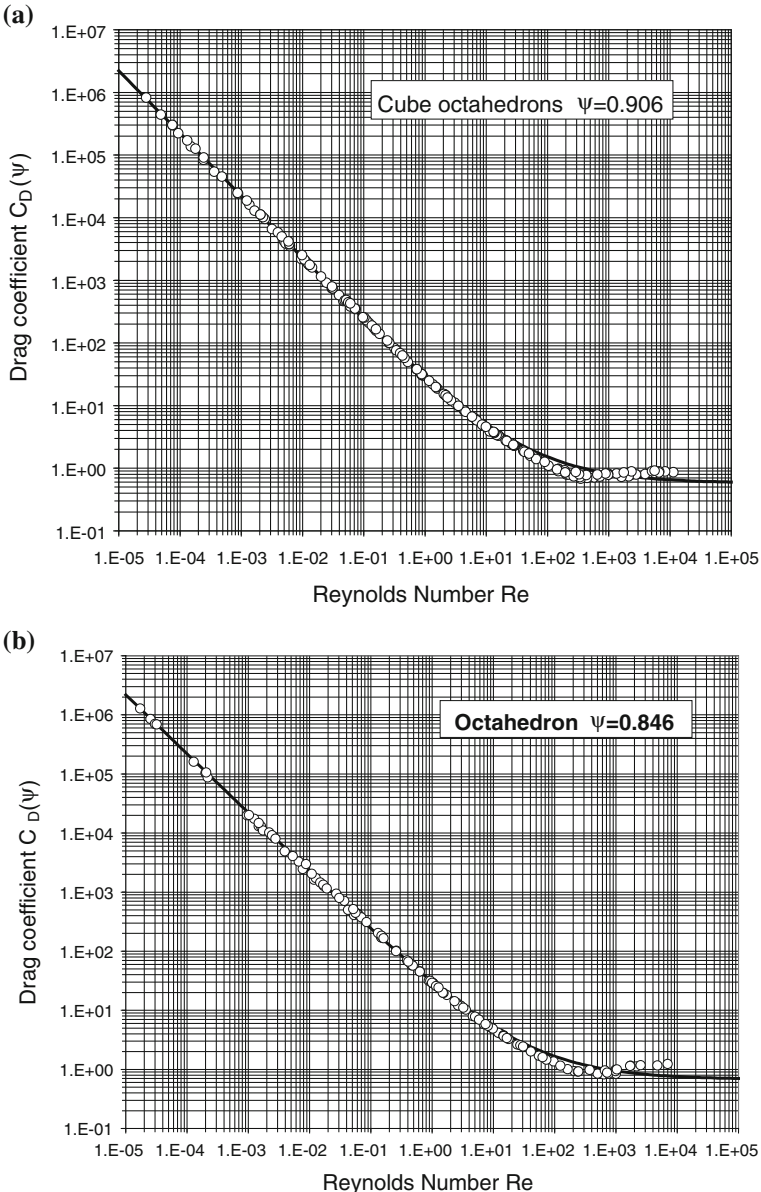


**Fig. 4.23** Simulation with Concha and Barrientos' equation (4.78) and experimental values for isometric particles from Pettyjohn and Christiansen (1948) and Barker (1951) for cube octahedrons (a), for octahedrons (b), for cubes (c), for tetrahedrons (d)

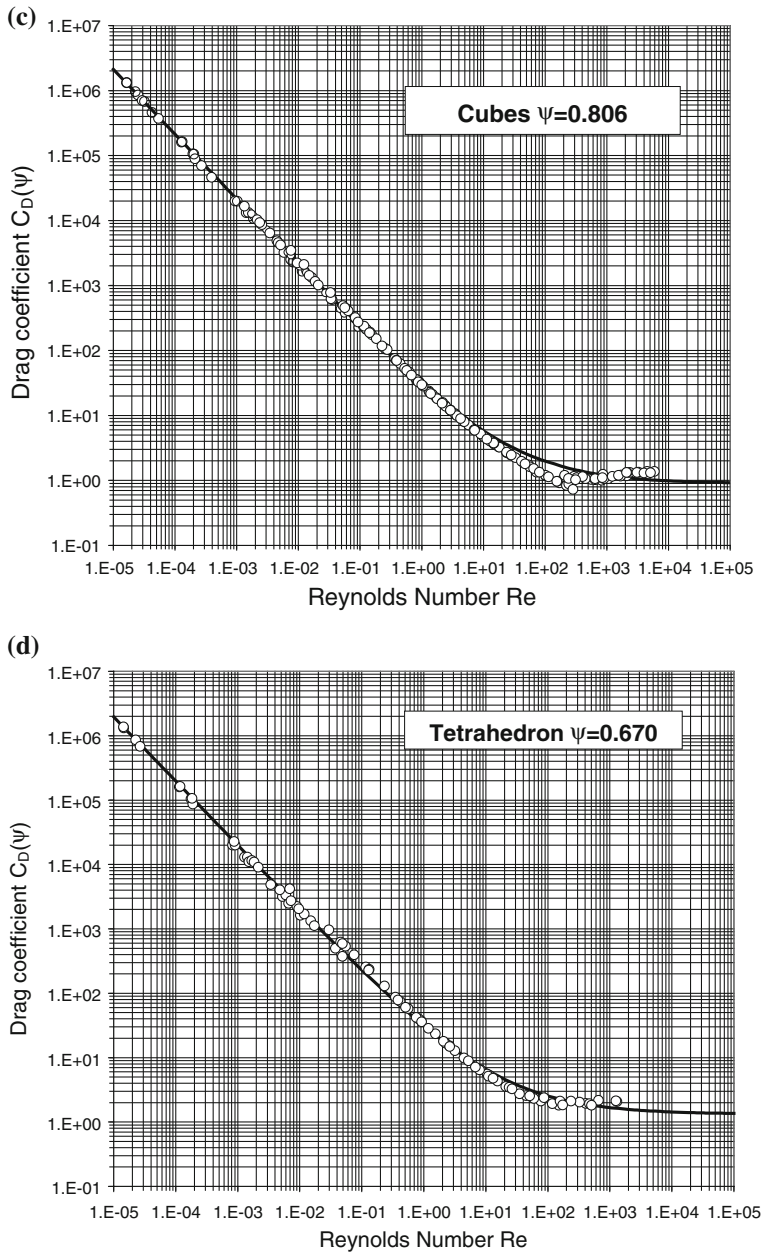


**Fig. 4.23** (continued)

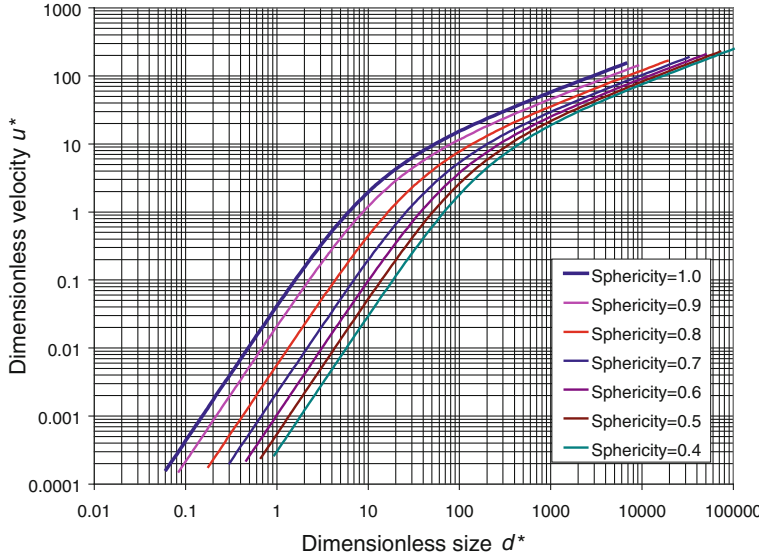


**Fig. 4.24** Dimensionles size versus dimensionless velocity for isometric particles according to Concha and Barrientos (1986)

$$C_D = \frac{1}{K_1} \frac{24}{\text{Re}} \left( 1 + 0.1118(K_1 K_2 \text{Re})^{0.6567} \right) + \frac{0.4305 K_1 K_2^2 \text{Re}}{3305 + K_1 K_2 \text{Re}} \quad (4.92)$$

where

$$K_1 = \left( \frac{1}{3} + \frac{2}{3} \psi^{-1/2} \right)^{-1}, \quad K_2 = 10^{1.8148(-\log \psi)^{0.5743}} \quad (4.93)$$

### Modified drag coefficient and sedimentation velocity

Introducing the values for  $f_A, f_B, f_C$  and  $f_D$  into Eq. (4.78) results in:

$$\frac{C_D(\psi, \lambda)}{f_A(\psi)f_C(\lambda)} = C_0 \left( 1 + \frac{\delta_0}{(\text{Re}/(f_B^2(\psi)f_D^2(\lambda)))^{0.5}} \right)^2 \quad (4.94)$$

Defining the modified Drag Coefficient  $C_{DM}$  and the modified Reynolds number  $\text{Re}_M$  by:

$$C_{DM} = \frac{C_D(\psi, \lambda)}{f_A(\psi)f_C(\lambda)} \quad \text{Re}_M = \left( \frac{\text{Re}}{f_B^2(\psi)f_D^2(\lambda)} \right) \quad (4.95)$$

we can write the drag coefficient in the form of Eq. (4.78). Plotting  $C_{DM}$  versus  $\text{Re}_M$ , Fig. 4.25 is obtained.

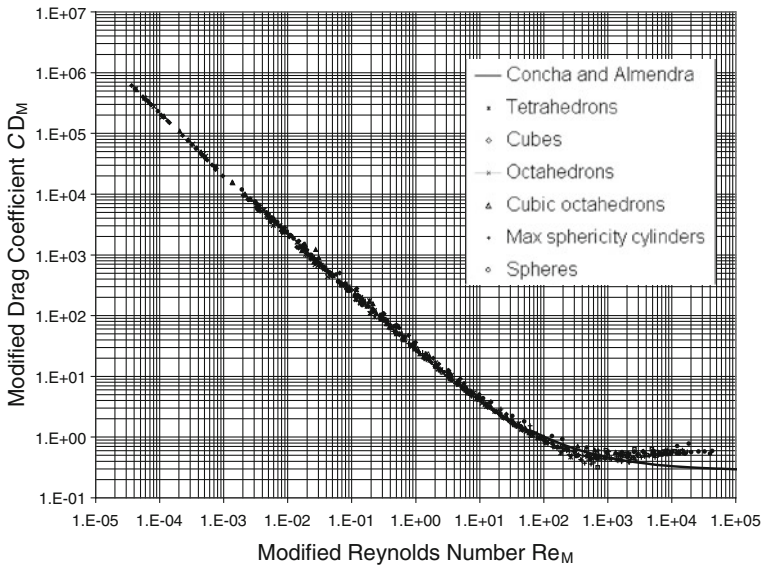


**Fig. 4.25** Experimental data of Pettyjohn and Christiansen (1948), and Barker (1951), plotted as  $C_{DM}$  versus  $Re_M$  for isometric particles

A similar result may be obtained for the sedimentation velocity. Defining modified dimensionless diameter  $d_{eM}^*$  and velocity  $u_M^*$ :

$$d_{eM}^* = \frac{d_e^*(\psi, \lambda)}{\left(f_A^{1/2}(\psi)f_B^2(\psi)f_C^{1/2}f_D^2(\lambda)\right)^{2/3}} \quad \text{and} \quad u_{eM}^* = \frac{u_p^*(\psi, \lambda)}{f_B(\psi)f_D(\lambda)}. \quad (4.96)$$

The unified  $u_{eM}^*$  versus  $d_{eM}^*$  curve is given in Fig. 4.26, for Pettyjohn and Christiansen (1948) and Christiansen and Barker (1965) data.

$$u_{eM}^* = \frac{20.52}{d_{eM}^*} \left( \left( 1 + 0.0921 d_{eM}^{3/2} \right)^{1/2} - 1 \right)^2 \quad (4.97)$$

The experimental data used in the previous correlations are 655 points including spheres, cubes-octahedrons, maximum sphericity cylinders, octahedrons and tetrahedrons in the following ranges:

$$\begin{aligned} 0.1 \text{ cm} &< d_e < 5 \text{ cm} \\ 1.7 \text{ g/cm}^3 &< \rho_s < 11.2 \text{ g/cm}^3 \\ 0.67 &< \psi < 1 \\ 0.87 \text{ g/cm}^3 &< \rho_f < 1.43 \text{ g/cm}^3 \\ 9 \times 10^{-3} \text{ g/cm s} &< \mu < 900 \text{ g/cm s} \\ 5 \times 10^{-3} &< Re < 2 \times 10^4 \end{aligned}$$

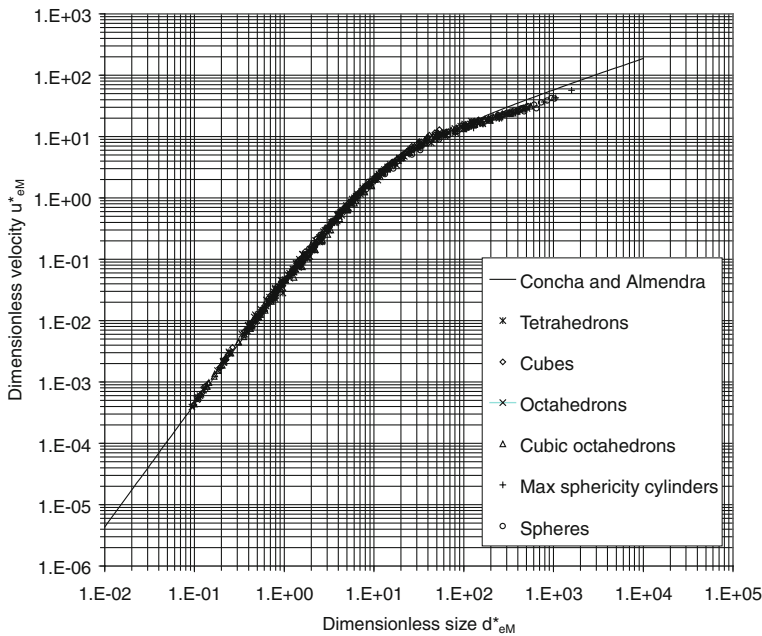


**Fig. 4.26** Unified  $u_M^*$  versus  $d_{eM}^*$  curve for data of Pettyjohn and Christiansen (1948) and Barker (1951)

with the following values for the particles sphericity (Happel and Brenner 1965; Barker 1951) and the parameters of Concha and Barrientos (1986)

	$\Psi$	$f_A(\psi)$	$f_B(\psi)$
Sphere	1.000	1.0000	1.0000
Cube octahec	0.906	1.4334	0.8826
Octahedron	0.846	1.9057	1.2904
Cube	0.806	2.2205	1.5468
Tetrahedron	0.670	3.2910	2.3108
Max sph cylin	0.875	1.6774	1.0966

**Problem 4.11** Determine the sphericity and the settling velocity of a quartz cube of 1 mm in size and a density of 2.65 g/cm<sup>3</sup> in water at 25 °C. Use the methods of Concha and Barrientos and that of Haider and Levenspiel.

By definition, sphericity is the ratio of the surface of a volume-equivalent sphere and the surface of the particle. For a cube of 1 mm in size, the surface is 6 mm<sup>2</sup> and its volume is 1 mm<sup>3</sup>. The volume equivalent sphere has a diameter of:

$$d_e = (6V/\pi)^{1/3} = (6/\pi)^{1/3} = (6/\pi)^{1/3}$$

The sphericity is:

$$\psi = \frac{\pi(6/\pi)^{2/3}}{6} = \left(\frac{\pi}{6}\right)^{1/3} = 0.806$$

Then, from Concha and Barrientos:

$$f_A(\psi) = \frac{5.31 - 4.88\psi}{0.62} = \frac{5.31 - 4.88 \times 0.806}{0.62} = 2.2205$$

$$f_B(\psi) = \left( \frac{5.31 - 4.88 \times 0.806}{0.62} \times 0.843 \log \frac{0.806}{0.065} \right)^{-1/2} = 0.699$$

$$\rho_{water} = -4.0 \times 10^{-6} \times 25^2 - 6.0 \times 10^{-5} \times 25 + 1.0004 = 0.9964 \text{ (g/cm}^3)$$

$$f_C(\psi) = \lambda^{-1/18} = \left( \frac{2.65}{0.9964} \right)^{-1/18} = 0.9471$$

$$f_D(\psi) = \lambda^{1/36} = \left( \frac{2.65}{0.9964} \right)^{1/36} = 1.0275$$

$$\tilde{\delta}_0(\psi, \lambda) = 9.08 \times f_B(\psi)f_D(\lambda) = 9.08 \times 0.699 \times 1.0275 = 6.5215$$

$$\tilde{C}_0(\psi, \lambda) = 0.28 \times f_A(\psi)f_C(\lambda) = 0.28 \times 2.2205 \times 0.9471 = 0.5889$$

$$\mu_{water} = 9.0 \times 10^{-7} \times 25^2 - 2.0 \times 10^{-4} \times 25 + 1.56 \times 10^{-2} = 0.0112 \text{ (g/cm} \times \text{s})$$

$$P = \left( \frac{3}{4} \frac{\mu_f^2}{\Delta \rho \rho_f g} \right)^{1/3} = \left( \frac{3 \times 0.0112^2}{4(2.65 - 0.9964) \times 0.9964 \times 980.1} \right)^{1/3} = 0.00387$$

$$Q = \left( \frac{4 \Delta \rho \mu_f g}{3 \rho_f^2} \right)^{1/3} = \left( \frac{4 \times (2.65 - 0.9964) \times 0.0112 \times 980.1}{3 \times 0.9964^2} \right)^{1/3} = 2.896$$

$$d^* = \frac{d_e}{P} = \frac{0.1}{0.00387} = 25.85$$

$$d_{eM}^* = \frac{d^*}{f_A^{0.5}(\psi)f_B^2(\lambda)f_C^{0.5}(\psi)f_D^2(\lambda)} = \frac{25.85}{2.2205^{0.5} \times 0.699^2 \times 0.9471^{0.5} \times 1.0275^2} \\ = 34.56$$

$$u_{eM}^* = \frac{20.52}{d_{eM}^*} \left( \left( 1 + 0.0921 d_{eM}^{*3/2} \right)^{1/2} - 1 \right)^2 = \frac{20.52}{40.67} \left( \left( 1 + 0.0921 \times 40.67^{3/2} \right)^{1/2} - 1 \right)^2 \\ = 7.025$$

$$u^* = u_{eM}^* f_B(\psi)f_D(\lambda) = 8.028 \times 0.699 \times 1.0275 = 5.046$$

$$u_p = Q \times u^* = 2.896 \times 5.046 = 14.61 \text{ cm/s}$$

Using the method of Haider and Levenspiel, Eq. (4.91), we get:

$$u_p^* = \left( \frac{18}{25.85^2} + \frac{3.1131 - 2.3252 \times 0.809}{25.85^{0.5}} \right)^{-1} = 3.6954$$

$$u_p = Q \times u_p^* = 2.89631 \times 3.694 = 10.703 \text{ cm/s}$$

### 4.1.9 Sedimentation of Particles of Arbitrary Shape

Concha and Christiansen (1986) extended the validity of Eqs. (4.78) and (4.79) to suspensions of particles of arbitrary shape.

$$C_D(\psi, \lambda, \varphi) = \tilde{C}_0(\psi, \lambda, \varphi) \left( 1 + \frac{\delta_0(\psi, \lambda, \varphi)}{Re^{1/2}} \right)^2 \quad (4.98)$$

$$u_p^*(\psi, \lambda, \varphi) = \frac{1}{4} \frac{\tilde{\delta}_0^2(\psi, \lambda, \varphi)}{d^*} \left( \left( 1 + \frac{4}{\tilde{C}_0^{1/2}(\psi, \lambda, \varphi) \tilde{\delta}_0^2(\psi, \lambda, \varphi)} d^{*3/2} \right)^{1/2} - 1 \right)^2 \quad (4.99)$$

where  $\psi$ ,  $\lambda$  and  $\varphi$  are the sphericity of the particles, the density ratio of solid and fluid and the volume fraction of solid in the suspension.

Similarly as in the case of isometric particles, they assumed that the functions  $\tilde{C}_0$  and  $\tilde{\delta}_0$  may be written in the form:

$$\tilde{C}_0(\psi, \lambda, \varphi) = C_0 f_A(\psi) f_C(\lambda) f_p(\varphi) f_q^{-2}(\varphi) \quad (4.100)$$

$$\tilde{\delta}_0(\psi, \lambda, \varphi) = \delta_0 f_B(\psi) f_D(\lambda) f_F(\varphi) f_p^{1/2}(\varphi) f_q^{1/2}(\varphi) \quad (4.101)$$

with

$$\begin{aligned} f_A(\psi) &= \frac{5.31 - 4.88\psi}{0.62} \\ f_B(\psi) &= \left\{ \frac{5.31 - 4.48\psi}{0.62} \times 0.843 \log \frac{\psi}{0.065} \right\}^{-1/2} \\ f_C(\lambda) &= \lambda^{1/18}, \quad f_D(\lambda) = \lambda^{-1/36} \\ f_p(\varphi) &= (1 - \varphi)^{-2.033}, \quad f_q(\varphi) = (1 - \varphi)^{-0.167} \end{aligned}$$

### Hydrodynamic shape factor

Concha and Christiansen (1986) found it necessary to define a *hydrodynamic shape factor* to be used with the above equations, since the usual methods to measure sphericity did not give good results. They defined the *effective hydrodynamic sphericity* of a particle as the *sphericity of an isometric particle having the same drag (volume) and the same settling velocity as the particle*.

The hydrodynamic sphericity may be obtained by performing sedimentation or fluidization experiments, calculating the drag coefficient for the particles using the volume equivalent diameter and obtaining the sphericity (defined for isometric particles) that fit the experimental value. Figure 4.27 give simulated Drag Coefficients curves for several sphericities.

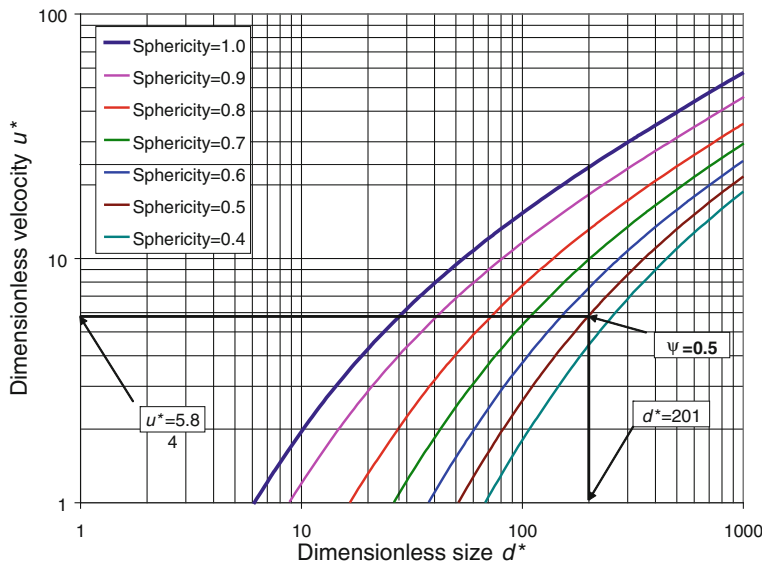


**Fig. 4.27** Simulated dimensionless velocity versus dimensionless size for isometric particles and several sphericities

**Problem 4.12** Estimate the sphericity of crushed quartz particle of 7.2 mm, with  $2.65 \text{ g/cm}^3$  in density, which gives an average settling velocity of 16.3 cm/s in water at  $20^\circ\text{C}$ .

$$d_e = 0.5 \text{ cm}, \rho_s = 2.65 \text{ g/cm}^3, \rho_f = 1.00 \text{ g/cm}^3, \mu = 0.01 \text{ g/cm s}$$

$$P = 0.00359, Q = 2.7921$$

Results:

$$d_e^* = \frac{d_e}{P} = \frac{0.72}{0.00359} = 2,001, u_p^* = \frac{u_p}{Q} = \frac{16.3}{2.7921} = 5.84$$

With these values for the equivalent dimensionless diameter and the dimensionless settling velocity of the particle  $d_e^*$  and  $u_p^*$ , from a plot of  $u^*$  versus  $d^*$ , see Fig. 4.27 we obtain a sphericity of  $\psi = 0.5$  for the quartz.

### Modified drag coefficient and sedimentation velocity

A unified correlation can also be obtained for the drag coefficient and the sedimentation velocity of irregular particles forming a suspension. Defining  $C_{DM}$ ,  $Re_M$ ,  $d_{eM}$  and  $u_{pM}$  in the following form:

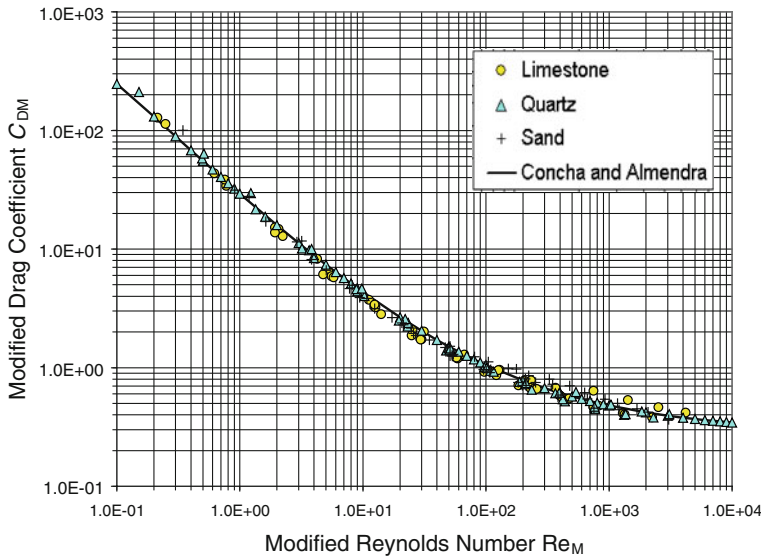


**Fig. 4.28** Unified drag coefficient versus Reynolds number for quartz, limestone and sand particles [the same data as in Fig. 4.22 (Concha and Christiansen 1986)]

$$C_{DM} = \frac{C_D(\psi, \lambda)}{f_A(\psi)f_C(\lambda)f_p(\varphi)} \quad Re_M = \left( \frac{Re}{f_B^2(\psi)f_D^2(\lambda)f_p^2(\varphi)} \right) \quad (4.102)$$

$$d_{eM}^* = \frac{d_e^*(\psi, \lambda)}{f_p(\varphi) \times \left( f_A(\psi)^{1/2} \times f_B^2(\psi) \times f_C(\lambda)^{1/2} \times f_D^2(\lambda) \right)^{2/3}} \quad (4.103)$$

$$u_{pM}^* = \frac{u_p^*(\psi, \lambda)}{f_B(\psi)f_D(\lambda)f_q(\varphi)} \quad (4.104)$$

Figures 4.28 and 4.29 show the unified correlations for the data from Concha and Christiansen (1986).

**Problem 4.13** Determine the minimum fluidization velocity of quartz particles with 250 microns in size, density  $\rho_s = 2.65 \text{ g/cm}^3$  and sphericity  $\psi = 0.55$ , in water and 20 °C.

The minimum fluidization velocity occurs at  $\varphi = 0.585$ , therefore, we have the following results:

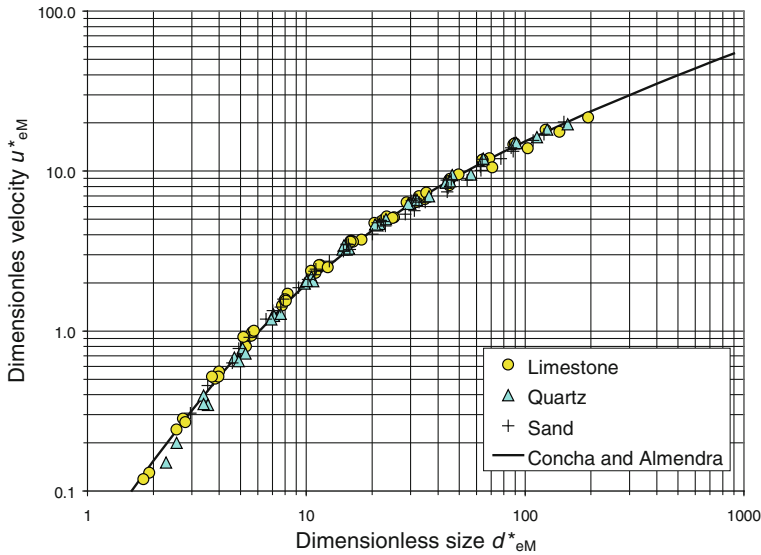


**Fig. 4.29** Unified sedimentation velocity versus size for limestone, quartz and sand particles [the same data as in Fig. 4.22 (Concha and Christiansen 1986)]

$$u^* = \frac{20.52}{d^*} f_p \times f_q \times f_B^2 \times f_D^2 \times \left( \left( 1 + \frac{0.0921 \times d^{*-3/2} f_p^{-3/2}}{f_A^{0.5} \times f_C^{0.5} \times f_B^2 \times f_D^2} \right)^{0.5} - 1 \right)^2$$

$$q = (1 - \varphi) \times u_p$$

$$\rho_s = 2.65 \text{ g/cm}^3$$

$$\rho_f = 1.09976 \text{ g/cm}^3, \quad \mu_f = 0.01196 \text{ g/cm - s}$$

$$P = 0.00405, \quad Q = 2.96151$$

$$f_A(\psi) = 4.2355, \quad f_B(\psi) = 0.5495, \quad f_C(\lambda) = 1.0558, \quad f_D(\lambda) = 0.9732$$

$$\varphi = 0.585, \quad f_p(\varphi) = 5.97734, \quad f_q(\varphi) = 1.1582.$$

$$d^* = d/P = 6.1737, \quad u^* = 0.03898, \quad u_p = u^* \times Q = 0.1154$$

$$q = (1 - \varphi) \times u_p = 0.04791 \text{ cm/s.}$$

Ganser (1993) proposed an empirical equation for the drag coefficient of non-spherical non-isometric particles, including irregular particles, similar to that given earlier for spherical particles (4.92), but with different values for the parameters  $K_1$ .

$$C_D = \frac{1}{K_1} \frac{24}{\text{Re}} \left( 1 + 0.1118(K_1 K_2 \text{Re})^{0.6567} \right) + \frac{0.4305 K_1 K_2^2 \text{Re}}{3305 + K_1 K_2 \text{Re}} \quad (4.105)$$

where

$$K_1 = \left( \frac{1}{3} \frac{d_p}{d_e} + \frac{2}{3} \psi^{-1/2} \right)^{-1}, \quad K_2 = 10^{1.8148(-\log \psi)^{0.5743}} \quad (4.106)$$

In the equation for  $K_1$ ,  $d_e$  and  $d_p$  are the *volume equivalent* and the *projected area* equivalent diameters of the irregular particle respectively.

Finally, it is interesting to mention the work of Yin et al. who analyzed the settling of cylindrical particles analytically and obtained, by linear and angular momentum balances, the forces and torques applied to the particle during their fall. Using Ganser's equation for the drag coefficient, they solved the differential equations of motion numerically obtaining results close to those measured experimentally by them.

## References

- Abraham, F. F. (1970). Functional dependence of the drag coefficient of a sphere on Reynolds number. *Physics of Fluids*, 13, 2194–2195.
- Barker, H. (1951). The effect of shape and density on the free settling rates of particles at high Reynolds Numbers, Ph.D. Thesis, University of Utah, Table 7, pp. 124–132; Table 9, pp. 148–153.
- Barnea, E., & Mitzrahi, J. (1973). A generalized approach to the fluid dynamics of particulate systems, 1. General correlation for fluidization and sedimentation in solid multiparticle systems. *Chemical Engineering Journal*, 5, 171–189.
- Barnea, E., & Mednick, R. L. (1975). Correlation for minimum fluidization velocity. *Transactions on Institute of Chemical Engineers*, 53, 278–281.
- Batchelor, G. K. (1967). *An introduction for fluid dynamics* (p. 262). Cambridge: Cambridge University Press.
- Brauer, H., & Sucker, D. (1976). Umströmung von Platten, Zylindern un Kugeln. *Chemie Ingenieur Technik*, 48, 665–671.
- Cabtree, L. F. (1963). Three dimensional boundary layers. In L. Rosenhead (Ed.), *Laminar boundary layers*, Oxford: Oxford University press, p. 423.
- Chabra, R. P., Agarwal, L., & Sinha, N. K. (1999). Drag on non-spherical particles: An evaluation of available methods. *Powder Technology*, 101, 288–295.
- Concha, F., & Almendra, E. R. (1979a). Settling velocities of particulate systems, 1. Settling velocities of individual spherical particles. *International Journal of Mineral Processing*, 5, 349–367.
- Concha, F., & Almendra, E. R. (1979b). Settling velocities of particulate systems, 2. Settling velocities of suspensions of spherical particles. *International Journal of Mineral Processing*, 6, 31–41.
- Concha, F., & Barrientos, A. (1986). Settling velocities of particulate systems, 4. settling of no spherical isometric particles. *International Journal of Mineral Processing*, 18, 297–308.
- Concha, F., & Christiansen, A. (1986). Settling velocities of particulate systems, 5. Settling velocities of suspensions of particles of arbitrary shape. *International Journal of Mineral Processing*, 18, 309–322.
- Christiansen, E. B., & Barker, D. H. (1965). The effect of shape and density on the free settling rate of particles at high Reynolds numbers. *AICHE Journal*, 11(1), 145–151.
- Darby, R. (1996). Determining settling rates of particles, *Chemical Engineering*, 109–112.
- Fage, A. (1937). Experiments on a sphere at critical Reynolds number (pp. 108, 423). London: Aeronautical Research Council, Reports and Memoranda, N°1766.

- Flemmer, R. L., Pickett, J., & Clark, N. N. (1993). An experimental study on the effect of particle shape on fluidization behavior. *Powder Technology*, 77, 123–133.
- Ganguly, U. P. (1990). On the prediction of terminal settling velocity in solids-liquid systems. *International Journal of Mineral Processing*, 29, 235–247.
- Ganser, G. H. (1993). A rational approach to drag prediction of spherical and non-spherical particles, 1993. *Powder Technology*, 77, 143–152.
- Goldstein, S. (Ed.). (1965). *Modern development in fluid dynamics* (Vols. 1, 2, p. 702). New York: Dover.
- Haider, A., & Levenspiel, O. (1998). Drag coefficient and terminal velocity of spherical and non-spherical particles. *Powder Technology*, 58, 63–70.
- Happel, J., & Brenner, H. (1965). Low Reynolds hydrodynamics (p. 220). NJ: Prentice-Hall Inc.
- Heywood, H. (1962). *Uniform and non-uniform motion of particles in fluids: Proceeding of the Symposium on the Interaction between Fluid and Particles*, Institute of Chemical Engineering, London, pp. 1–8.
- Lapple, C. E., & Shepherd, C. B. (1940). Calculation of particle trajectories. *Industrial and Engineering Chemistry*, 32, 605.
- Lee, K., & Barrow, H. (1968). Transport process in flow around a sphere with particular reference to the transfer of mass. *International Journal of Heat and Mass Transfer*, 11, 1020.
- Lighthill, M. J. (1963). Boundary layer theory. In L. Rosenhead (Ed.), *Laminar boundary layers*, Oxford: Oxford University, p. 87.
- Massarami, G. (1984). Problemas em Sistemas Particulados, Blücher Ltda., Rio de Janeiro, Brazil, pp. 102–109.
- McDonald, J. E. (1954). *Journal of Applied Meteorology*, 11, p. 478.
- Meksyn, D. (1961). New methods in boundary layer theory, New York.
- Newton, I. (1687). *Filosofiae naturalis principia mathematica*, London.
- Nguyen, A. V., Stechemesser, H., Zobel, G., & Schulze, H. J. (1997). An improved formula for terminal velocity of rigid spheres. *International Journal of Mineral Processing*, 50, 53–61.
- Richardson, J. F., & Zaki, W. N. (1954). Sedimentation and fluidization: Part I. *Transactions on Institute of Chemical Engineers*, 32, 35–53.
- Perry 1963, p. 5.61.
- Pettyjohn, E. S., & Christiansen, E. B. (1948). Effect of particle shape on free-settling of isometric particles. *Chemical Engineering Progress*, 44(2), 157–172.
- Rosenhead, L. (ed) (1963). *Laminar boundary layers* (pp. 87, 423, 687). Oxford: Oxford University Press.
- Schlichting, H. (1968). *Boundary layer theory*. New York: McGraw-Hill. 747.
- Stokes, G. G. (1844). On the theories of internal friction of fluids in motion and of the equilibrium and motion of elastic solids. *Transactions on Cambridge Philosophical Society*, 8(9), 287–319.
- Taneda, S. (1956). *Rep. Res. Inst. Appl. Mech.*, 4, 99.
- Thomson, T., & Clark, N. N. (1991). A holistic approach to particle drag prediction. *Powder Technology*, 67, 57–66.
- Tomotika, A.R.A. (1936). Reports and memoranda N°1678, See also Goldstein 1965, p. 498.
- Tory, E. M. (1996). *Sedimentation of small particles in a viscous fluid*. UK: Computational Mechanics Publications Inc.
- Tsakalis, K. G., & Stamboltzis, G. A. (2001). Prediction of the settling velocity of irregularly shaped particles. *Minerals Engineering*, 14(3), 349–357.
- Tourton, R., & Clark, N. N. (1987). An explicit relationship to predict spherical terminal velocity. *Powder Technology*, 53, 127–129.
- Tourton, R., & Levenspiel, O. (1986). A short Note on the drag correlation for spheres. *Powder Technology*, 47, 83–86.
- Wadell, J. (1932). Volume shape and roundness of rock particles, *Journal of Geology*, 15, 43–451.

- Wadell, J. (1934). The coefficient of resistance s a function of the Reynolds number for solids of various shapes, *Journal of the Franklin Institute* 217, 459–490.
- Zens, F. A., & Othme, D. F. (1966). Fluidization and fluid-particle systems. New York: McGraw-Hill.
- Zigrang, D. J., & Sylvester, N. D. (1981). An explicit equation for particle settling velocities in solid-liquid systems. *AICHE Journal*, 27, 1043–1044.